International Journal of Earth Sciences

Role of transverse structures in paleoseismicity and drainage rearrangement in rift systems: the case of the Valdecebro fault zone (Teruel graben, eastern Spain)

--Manuscript Draft--

Manuscript Number:	
Full Title:	Role of transverse structures in paleoseismicity and drainage rearrangement in rift systems: the case of the Valdecebro fault zone (Teruel graben, eastern Spain)
Article Type:	Original Paper
Keywords:	active fault, paleoearthquake, biaxial extension, OSL dating, drainage capture
Corresponding Author:	José Luis Simón, Ph.D. Universidad de Zaragoza Zaragoza, Zaragoza SPAIN
Corresponding Author Secondary Information:	
Corresponding Author's Institution:	Universidad de Zaragoza
Corresponding Author's Secondary Institution:	
First Author:	José Luis Simón, PhD
First Author Secondary Information:	
Order of Authors:	José Luis Simón, PhD
	Lope Ezquerro, PhD
	Luis Eduardo Arlegui, PhD
	Carlos Luis Liesa, PhD
	Aránzazu Luzón, PhD
	Alicia Medialdea, PhD
	Alberto García, Graduate
	Daniel Zarazaga, Graduate
Order of Authors Secondary Information:	
Funding Information:	Ministerio de Economía, Industria y Competitividad, Gobierno de España (CGL2012-35662) — Dr José Luis Simón
Abstract:	The E-W trending, nearly pure extensional Valdecebro fault zone is a transverse structure at the central sector of the N-S Teruel graben. It was activated by the late Ruscinian (Early Pliocene, ca. 3.7 Ma), giving rise to structural rearrangement of the graben margin. Until the Late Pleistocene, it has accommodated a net slip ca. 205 m, with slip rate of 0.055 mm/a. Paleoseismicity has been analysed in a 29-m-long, 5-m-deep trench excavated through a fault branch that offsets a Pleistocene pediment surface. The paleoseismic succession includes a minimum of six-seven events occurred since ca. 142 ka BP, although a model with twelve events could be more realistic. The following paleoseismic parameters have been inferred: average coseismic slip = 58-117 cm; recurrence period = 8.4-28.4 ka; potential moment magnitude Mw = 5.8-5.9. The recorded displacement since ca. 142 ka BP totalizes 7.0 m, with slip rate of 0.05-0.07 mm/a. Slip on the transverse Valdecebro fault zone has critically contributed to bulk deformation under a prevailing 'multidirectional' extensional regime. Drainage patterns have been rearranged, recurrently switching between westward and southward directions as a consequence of diverse slip episodes at the Valdecebro fault zone (E-W) and the neighbouring La Hita (N-S) and Concud (NW-SE) faults. The ultimate westward drainage of the Valdecebro depression incised and dismantled a southward sloping Pleistocene pediment sourced at the Valdecebro

	mountain front, representing a capture by the Alfambra river occurred between 124 and 22 ka BP.

Role of transverse structures in paleoseismicity and drainage rearrangement in rift systems: the case of the Valdecebro fault zone (Teruel graben, eastern Spain)

José L. Simón[a]*, Lope Ezquerro[a], Luis E. Arlegui[a], Carlos L. Liesa[a], Aránzazu Luzón[a], Alicia Medialdea[b], Alberto García[c], Daniel Zarazaga[d]

[a] Departamento de Ciencias de la Tierra & Instituto de Ciencias Ambientales (IUCA), Facultad de Ciencias, Universidad de Zaragoza, Pedro Cerbuna 12, 50009 Zaragoza, Spain
[b] Geographisches Institut, Universität zu Köln, Otto-Fischer-Str. 4, 50674 Köln, Germany
[c] CTA, Consultores Técnicos Asociados S.A., C/ Fray Luis Amigó, 8, 50009 Zaragoza, Spain.
[d] C/ Julio García Condoy, 36, 1 B, 50018 Zaragoza, Spain

* Corresponding author: E-mail: jsimon@unizar.es. Tel.: +34 976 76 10 95. ORCID: 0000-0003-1412-5245

ABSTRACT

The E-W trending, nearly pure extensional Valdecebro fault zone is a transverse structure at the central sector of the N-S Teruel graben. It was activated by the late Ruscinian (Early Pliocene, ca. 3.7 Ma), giving rise to structural rearrangement of the graben margin. Until the Late Pleistocene, it has accommodated a net slip ca. 205 m, with slip rate of 0.055 mm/a. Paleoseismicity has been analysed in a 29-m-long, 5-m-deep trench excavated through a fault branch that offsets a Pleistocene pediment surface. The paleoseismic succession includes a minimum of six-seven events occurred since ca. 142 ka BP, although a model with twelve events could be more realistic. The following paleoseismic parameters have been inferred: average coseismic slip = 58-117 cm; recurrence period = 8.4-28.4 ka; potential moment magnitude Mw = 5.8-5.9. The recorded displacement since ca. 142 ka BP totalizes 7.0 m, with slip rate of 0.05-0.07 mm/a. Slip on the transverse Valdecebro fault zone has critically contributed to bulk deformation under a prevailing ‘multidirectional’ extensional regime. Drainage patterns have been rearranged, recurrently switching between westward and southward directions as a consequence of diverse slip episodes at the Valdecebro fault zone (E-W) and the neighbouring La Hita (N-S) and Concud (NW-SE) faults. The ultimate westward drainage of the Valdecebro depression incised and dismantled a southward sloping Pleistocene pediment sourced at the Valdecebro mountain front, representing a capture by the Alfambra river occurred between 124 and 22 ka BP.

***Keywords*:** active fault, paleoearthquake, biaxial extension, OSL dating, drainage capture.

1. Scope and objectives

It is known that paleoseismic reconstructions are critical for assessing seismic hazard in areas of low-rate tectonic activity, where the time window covered by the historical record is not long enough to include large earthquakes. But Paleoseismicity also contributes to tectonic knowledge, providing detailed kinematical information of active faults, specifically its pattern of incremental slip (Simón *et al.*, 2017).

This is the case of eastern Iberian Chain (eastern Spain), an intraplate region that contains a number of large active extensional faults, although it shows low instrumental and historical seismicity. The intra-mountain Teruel and Jiloca grabens constitute the largest Neogene-Quaternary extensional structures in the region, controlled by faults that follow two prevailing directions: N-S to NNE-SSW, and NW-SE to NNW-SSE, respectively. The NW-SE striking Concud fault and the N-S striking Teruel fault are the main active structures at the junction of the Teruel and Jiloca grabens (Fig. 1). Both faults have been studied from the structural and paleoseismological point of view, evincing recurrent, seismogenic displacement during the Late Pleistocene (Lafuente, 2011; Lafuente *et al.*, 2011a, 2014; Simón *et al.*, 2016, 2017). The target of this study, the Valdecebro fault zone, has not been object of any specific study up to present. It is located at the central sector of the Teruel basin, close to its eastern boundary, and exhibits a nearly E-W direction that sharply contrasts with the nearly N-S trend of the Teruel graben.

Such structural setting is consistent with the recent, Pliocene-Quaternary stress regime at the eastern Iberian Chain: biaxial or 'multidirectional' extension (σ_1 vertical, $\sigma_2 \approx \sigma_3$) (Simón, 1989; Arlegui *et al.*, 2005). According to the notion of *strain/stress partitioning* (Simón *et al.*, 2008), biaxial extensional deformation could be accommodated by slip on faults of diverse orientations, through a non-linear sequence of rupture episodes linked to systematic, not chaotic stress changes (stress deviation, stress switching; Simón *et al.*, 1988; Caputo, 1995, 2005; Kattenhorn *et al.*, 2000; Bai *et al.*, 2002). Since each slip event can be considered as geologically 'instantaneous', paleoseismology provides a useful tool for analysing incremental deformation within a narrow time window.

This paper presents the results of a structural and paleoseismological study of the Valdecebro fault zone. The paleoseismic succession reconstructed from trench study will contribute to improve seismic assessment in the Teruel area. Moreover, structural and seismogenic parameters of the Valdecebro fault zone will be included into the QUAFI database (Quaternary Active Fauts Database of Iberia; http://info.igme.es/qafi/), with the purpose of contributing to overall seismic hazard assessment of Spain.

On the other hand, activation of the anomalous E-W trending Valdecebro fault zone gave rise to strong rearrangement of the formerly N-S trending basin margin, and hence readjustment of drainage and sedimentation systems. Also these aspects are explored, in order to understand relationships between structural development and changes in landscape and drainage network in complex extensional basins.

In summary, our specific objectives are the following:

(1) Reconstructing recent activity of the Valdecebro fault zone and its paleoseismic record, and comparing them with the neighbouring Concud and Teruel faults.

(2) Reconstructing drainage changes linked to the onset of the Valdecebro fault zone.

(3) Integrating its structural and morphotectonic evolution into a synthetic model of basin margin readjustment.

2. Methodology

First, a geological and morphotectonic study of the area surrounding the Valdecebro fault zone was carried out. It was based on the usual techniques such as field survey, analysis of orthoimages and stereoscopic aerial photographs, complemented with topographic data: UTM coordinates adquired by means of GPS (Garmin Oregon 450); height measurements of critical markers (Nikon hypsometer Forestry 550 pro), and a laser-level profile along a gentle fault scarp (Leica Sprinter 100). Detailed geologic and morphotectonic maps of the area were elaborated, together with height profiles of pediments and stream channels, and calculations of the Stream-gradient index (*SL*; Hack, 1973).

The optimum location for trench study was selected from that geological, geomorphological and topographical information. The target was a surficial rupture that produced a visible, anomalous topographical step on a pediment surface. A trench was dug orthogonal to it, with the purpose of exposing one or several fault surfaces, as well as recent sediments affected by them. We applied the classical procedure (e.g., McCalpin, 1996) including: cleansing and gridding trench walls; identifying and marking sedimentary units and structures; drawing a detailed log and taking photographs of each grid cell; analysing the relationships between units and faults to identify individual events; and collecting samples for absolute dating of sedimentary units, and hence constraining the ages of paleoseismic events.

Chronology of the sedimentary units has been established on the basis of sample dating using Optically Stimulated Luminescence (OSL). A total of six samples were collected using opaque tubes to avoid exposure to daylight, then processed at the Unit of Radioisotopes at the University of Seville, Spain. The luminescence signal was measured on the quartz fractions of sizes 180-250 μm extracted from each sample. The single aliquot regenerative dose (SAR) protocol (Murray and

Wintle, 2003) was applied for all measurements. Equivalent doses (D_e) were determined by interpolating the natural luminescence signal on the corresponding corrected dose response curve. A dose recovery test at preheat temperatures ranging from 180ºC to 260 ºC was performed on one of the samples (VAL47F) to determine the most appropriate. Based on this test, a preheat temperature of 200°C for 10 s and cutheat temperature of 180°C, both at 5°C/s, have been used for all luminescence measurements unless otherwise stated. Further methodological details will be given while explaining the results in Section 6.3.

3. Geological setting

The Neogene-Quaternary extensional basins of the eastern Iberian Chain (Fig. 1) represent the onshore deformation of the Valencia trough (Roca and Guimerà 1992). Faults controlling those basins are broadly parallel to the S_{Hmax} (maximum horizontal stress) directions characterizing the stress systems prevailing during Neogene-Quaternary times in eastern Spain: intraplate NNW-SSE compression produced by Africa-Iberia convergence, and WNW-ESE extension induced by rifting at the Valencia trough (Simón, 1982, 1983). Superposition of both stress systems, together with extension induced by recent, Late Pliocene-Quaternary crustal doming at the central-eastern Iberian Chain, have resulted in a complex, fluctuating and evolving regional stress field. Triaxial extension with σ_3 trajectories oriented W-E to WNW-ESE prevail during a first rift episode, mainly Late Miocene in age; biaxial or 'multidirectional' extension with σ_3 trending nearly WSW-ENE characterizes a second, Pliocene-Quaternary one (Simón, 1982, 1989; Arlegui *et al*., 2005), remaining active up to the present-day (Herraiz *et al*., 2000).

The Teruel basin is a half graben whose active, eastern boundary shows prominent, N-S to NNE-SSW trending mountain fronts that separate the bottom (usually at 800-1000 m a.s.l.) from El Pobo, Camarena and Javalambre ranges (between 1600 and 2000 m). This basin is filled with Neogene red alluvial deposits that grade basinwards into lacustrine evaporites and carbonates. Several litostratigraphic (Godoy *et al*., 1983) or genetic (Alcalá *et al*., 2000; Ezquerro, 2017) units have been defined. Their ages, well constrained by means of numerous mammal fossil localities and magneto-stratigraphic studies, range from the early Late Miocene (Vallesian) to the Late Pliocene-earliest Pleistocene (Villafranchian) (Alcalá *et al*., 2000; Ezquerro, 2017)

Mountains surrounding the Teruel basin show two main planation surfaces modelling Mesozoic rocks: *Intramiocene Erosion Surface* (*IES*; Gutiérrez and Peña, 1976; Peña *et al*., 1984), which makes the summits of the highest bounding reliefs (ca. 1600 to 1750 m a.s.l.), and *Fundamental Erosion Surface* (*FES*, Peña *et al*., 1984), which makes vast platforms at intermediate heights (usually ca. 1250-1500 m). Within the Teruel basin, *IES* and *FES* correlate, respectively, with the basal unconformity of the Neogene infill and the top of the *Páramo 2* unit, being dated to 11.2 Ma and 3.7-3.5 Ma, respectively (Ezquerro, 2017).

During Late Pliocene-Quaternary times the Neogene infill of the Teruel basin was deeply excavated by the Alfambra and Turia rivers and their tributaries. Four main fluvial terrace levels are identified (Peña, 1981; Godoy *et al*., 1983), some of them locally splitting into several sublevels (Sánchez Fabre, 1989; Moissenet, 1993). The Middle and Lower terraces are persistent, lying between 45-65 m and 10-15 m above talwegs, with numerical ages ranging from 250 ± 32 to 15 ± 1 ka (Sánchez Fabre, 1989; Moissenet, 1993; Arlegui *et al*., 2005; Gutiérrez *et al*., 2008; Lafuente, 2011; Simón *et al*., 2016, 2017). Finally, a Holocene terrace level at 3-5 m above the talweg has been dated to 3.4 ± 0.7 ka (Lafuente, 2011; Lafuente *et al*., 2014).

Five main recent extensional faults have controlled the tectonic evolution of the Teruel graben at its junction with the Jiloca graben: Concud, Teruel, Tortajada, La Hita and Valdecebro faults (Fig. 1). The Concud fault is the most documented active structure in the region (*e.g*. Lafuente, 2011; Lafuente *et al*., 2011a, 2014; Simón *et al*., 2016). It is a NW-SE trending fault with average transport direction towards N220ºE. Its accumulated net displacement for the overall extensional history (since latest Ruscinian, 3.5 Ma; Ezquerro, 2017) is estimated within the range of 255-290 m, resulting in a net slip rate of 0.07-0.08 mm/a (Lafuente, 2011; Lafuente *et al*., 2011a). Paleoseismological studies indicate that it underwent eleven events since ca. 74 ka BP, with an average recurrence period of 7.1- 8.0 ka and average coseismic slip of 1.9 m. The slip history shows alternating periods of fast (up to 0.53 mm/a) and slow (0.13 mm/a) slip, resulting in average net slip rate of 0.29 mm/a (Simón *et al*., 2016).

Also the Teruel fault has shown a remarkable activity, although its paleoseismic record is much poorer. It is a N-S trending fault with average transport direction towards N275ºE, accumulated net displacement of ca. 270 m since 3.5 Ma, and net slip rate of 0.075 mm/a (Ezquerro, 2017; Simón *et al*., 2017). Its limited paleoseismic record includes four events occurred between 76.0 and 9.2 ka BP in two fault branches, involving a limited slip rate of ca. 0.04 mm/a calculated from trench analysis, which could increase up to ca. 0.19 ± 0.01 mm/a seeing at the displacement of a dated terrace level (8.8 m since 46.5 ± 3.2 ka; Simón *et al*., 2017). The Concud and Teruel faults make a right, 1.3-km-wide relay zone, while show no structural link and behave as kinematically independent structures with distinct transport directions (Lafuente *et al*., 2011b).

The Tortajada fault and La Hita fault zone are less known, particularly their Quaternary activity. The Tortajada fault strikes NNE-SSW, separating the central sector of the Teruel basin from the intermediate Corbalán block (Fig. 1). It was activated during the middle Turolian (Late Miocene, ca. 6.1 Ma), long after the overall Teruel graben was set up (Ezquerro, 2017). Its total net slip is estimated at ca. 370 m, while the post-*FES* slip approaches 275 m. The resulting average slip rate is 0.06 mm/a since 6.1 Ma BP, and 0.08 mm/a since 3.7-3.5 Ma BP. The N-S trending La Hita fault zone makes the central segment of the basin margin, and is virtually the only one that was active since graben initiated ca. 11.2 Ma ago (Ezquerro, 2017). North of this segment, a gentle monocline represented the diffuse margin until being shifted to the Tortajada fault. The total net slip of La Hita fault zone is estimated at 700 m, while the post-*FES* slip is ca. 265 m. The resulting average slip rates are 0.06 mm/a (since 11.2 Ma), and 0.075 mm/a (since 3.7-3.5 Ma ago).

Historic and instrumental seismicity of the Teruel basin and the surrounding region is low to moderate. Epicentres are concentrated along N-S striking faults south of Teruel city, western margin of the Jiloca graben and its neighbouring Albarracín Massif. The maximum recorded magnitude is Mb = 4.4 (IGN, 2010). Focal depths typically correspond to the brittle layer above the basal, 10-15 km deep detachment level identified by Roca and Guimerà (1992). Most of the available focal mechanisms correspond to normal faults and are consistent with the recent stress field (Herraiz *et al*., 2000).

4. The Valdecebro area

The E-W trending Valdecebro fault zone makes the northern boundary of a topographic depression, and separates it from the upthrown Corbalán block located to the north (Fig. 2a). The elongated, E-W trending Valdecebro depression represents a marginal corner of the Teruel graben. It is closed at its western end by the Mansuetos mesa, and is drained westwards by the Río Seco gully. At its eastern sector, it is dominated by a huge Villafranchian pediment sourced at La Hita mountain front. The Valdecebro depression has a mixed origin: it primarily represents a gentle half-graben inserted into the central Teruel graben, produced by rollover bending associated to the Valdecebro fault zone (Ezquerro, 2017); however, its final relief has been mainly acquired by differential erosion of soft Neogene materials with respect to the hard Jurassic rocks of the Corbalán block (Sánchez Fabre, 1989).

4.1. Materials

Neogene and Quaternary materials are well exposed in the Valdecebro depression. The Neogene infill is mainly composed of red clastic deposits and whitish-grey carbonates, and the stratigraphic architecture draws a paleogeographical sketch with alluvial fans mainly coming from the E and NE and grading downstream into lacustrine-palustrine areas (Ezquerro, 2017). The informal lithostratigraphic units defined by Godoy *et al*. (1983) can be recognized:

- *Lower Clastic* unit and *Rojo 1* unit (Vallesian). Red mudstone with interbedded tabular or channelled conglomerate bodies. They represent middle-distal sectors of large alluvial fans sourced in the NE and E margins. In the western sector (Los Mansuetos), both units are separated by the *Intermediate Limestone* unit (Vallesian), made of lacustrine-palustrine carbonates.

- *Páramo 1* unit (Turolian). Whitish limestone and marl in tabular strata with gastropods, vegetal remains and root traces, representing lacustrine-palustrine sedimentation.

- *Rojo 2* unit (Turolian-Ruscinian). Red sandstone and mudstone with interbedded channelled conglomerate bodies and palaeosoils.

- *Páramo 2* unit (Ruscinian). Grey limestone and marl in tabular or irregular cm- to m-thick beds, exhibiting abundant fossils (gastropods, ostracods, charophytes and vegetable remains) typical of lacustrine-palustrine environments.

- *Rojo 3* unit (Ruscinian). Grain-supported conglomerate with polygenic clasts, interbedded with decimetric sandstone and silt tabular beds. It represents proximal to middle sectors of alluvial fans mainly sourced at the East, finally capped by the *Villafranquian Pediment* (Gutiérrez and Peña, 1976; Godoy *et al*., 1983).

Within this Neogene succession, Ezquerro (2017) has defined six, TN1 to TN6 genetic units (mapped in Fig. 2a; see correlation with informal units by Godoy *et al*., 1983 in Fig. 2b), representing successive episodes of retrograding-prograding evolution of the alluvial systems. Alluvial progradation are generally linked to episodes of higher tectonic activity, except in the case of the limit between TN2 and TN3, whose prograding setup is related to a change towards drier conditions (Ezquerro *et al*., 2014; Ezquerro, 2017).

Quaternary deposits consist of matrix-supported gravels with mainly carbonate, subrounded to angular pebbles and silty to sandy matrix. The thicker (up to 10 m-thick) and wider deposits represent alluvial systems sourced at the northern margin and modelled into pediment surfaces. Thinner gravel accummulations fill the present-day alluvial plain of the Río Seco gully.

4.2. Structure

The Valdecebro fault zone is an intrabasinal, 5.2 km-long structure made of a number of extensional faults striking E-W to ESE-WNW (Fig. 2a,c). It extends between the Triassic outcrop of Tortajada, to the west, and the N-S trending Rambla del Burro faults, to the east. The latter belong to a complex fault network that extends southwards cutting the Villafranchian pediment (with NNW-SSE, WNW-ESE and N-S orientations), and is associated to the N-S trending La Hita fault zone. Some ruptures within the Valdecebro fault zone, mainly those at the western sector, yuxtapose Upper Miocene conglomerates of the Valdecebro depression against Jurassic limestones of the upthrown Corbalán block. To the east, these conglomerates onlap the basin margin, while a number of faults cut Miocene units of the hanging-wall block.

Neogene deposits show flat layers, lying horizontal at the southern sector and slightly dipping towards the north at the northern one, therefore making a gentle rollover anticline (Fig. 2d). Within the fault zone, ruptures are both synthetic and antithetic with respect to the structural step, therefore exhibiting a horst-and graben style. Locally, southward drag tilting is observed in Miocene beds close to synthetic faults. Fault surfaces exposed at a number of sites (see location in Fig. 2a) strike around WNW-ESE, and dip moderately to steeply (range from 46 to 86º, average = 69º), towards N and S. Striations indicate nearly pure normal movement: pitch 85ºW on a plane representative of the modal orientation N106ºE, 62ºS; transport direction of the hanging wall towards N202ºE (Fig. 2c).

Activity of the Valdecebro fault zone is documented from Early Pliocene to Late Pleistocene times. As inferred from facies distribution of the Neogene units and their relationships with the macrostructures, the fault did not have any imprint on sedimentation during Vallesian and Turolian times. It begun to move giving rise to a new basin margin in the late Ruscinian (megasequential boundary B4 defined by Ezquerro, 2017, ca. 3.7 Ma), and remained active during the Villafranchian. Some of the surficial ruptures were then overlaid by Pleistocene pediment deposits, while others cut and offset such pediments revealing later activity.

4.3. Landforms

The Valdecebro depression shows three sectors dominated by three distinctive landforms (Sánchez Fabre, 1989) (Fig. 3a):

- Eastern Villafranchian pediment. It comes from the Cabezo Alto mountain front, its altitude diminishing from 1240 to 1160 m a.s.l. (slope 2-3%). The surface lies 70-100 m higher than the talweg of Río Seco gully. Its relative height and slope are strongly distorted by the fault network referred in Section 4.2 and represented in maps of Figures 2a and 3a.
- Northern Pleistocene pediments. The main pediment system comes from the E-W trending Valdecebro fault scarp (Fig. 3b), starting at heights of 1180 (east) to 1120 m (west) and extending southwards up to lie below 1050 m at the southern sector of the study area. It shows a slope in the range of 3-6% and lies 40-60 m higher than the Río Seco talweg. A secondary pediment system comes from the Mansuetos mesa, at the SW corner of Figure 3a, and goes downslope towards SE converging with the former one.
- Central Río Seco valley. The Río Seco gully has excavated the soft Neogene materials of the central Valdecebro depression. It occupies a wide, flat-bottom valley made of a Holocene pediment in which the present-day gully is incised 4-6 m.

At its origin, the southward sloping pediment system was not tributary of the axial drainage of the Valdecebro depression (Río Seco gully); on the contrary, it extended southwards beyond the gully and finally connected with another drainage system tributary of the Turia river (out of Fig. 3a). The height profile represented in Figure 3c illustrates such paleotopographic setting. In consequence, the Río Seco drainage represents a relatively young, westward capture of a depression that originally was drained to the south. The time of this capture event can be constrained between ca. 124 ka BP, the most recent age of the functional pediment deposits (i.e. youngest vestige of prevailing southward drainage, according to numerical ages provided in the present work; see Section 6.4), and 22.0 ± 1.6 ka, the age of the oldest terrace level of the Río Seco gully near its confluence with the Alfambra river (i.e. first vestige of westward drainage; Simón *et al*., 2016).

The topographic depression is surrounded by higher reliefs dominated by older, Neogene erosional and depositional surfaces (Fig. 3a). To the west, it is barred by the Mansuetos mesa, which is caped by the *Páramo 2* lacustrine unit. To the north and east, the Jurassic rocks of the Corbalán and Cabezo Alto blocks are levelled by the *Fundamental Erosion Surface* (*FES*; Peña *et al*., 1984), whose achievement is correlative of the *Páramo 2* top (in our study area, the top of the Mansuetos series, ca. 3.7 Ma; Ezquerro, 2017). Owing to recent deformation, this planation surface is located at variable heights (see contours in Fig. 3a).

5. Assessing overall activity of the Valdecebro fault zone

5.1. Morphotectonic approach

The Valdecebro fault zone is expressed in the landscape by a gentle fault-generated mountain front 50 to 100 m high and some 4.5 km long (Figs. 3b, 4a). This is dissected by transverse stream channels belonging to different categories according to their length and development of their drainage basins (Fig. 4a): (I) major, plurikilometre-scale gullies, whose drainage basins largely enter the Corbalán block exhibiting a dendritic pattern (numbers 5, 18 and 22 in Fig. 4a); (II) middle, kilometre-scale gullies whose drainage basins show limited entrance into the upthrown block (1, 8, 14, 15, 16); (III) more abundant hectometre-scale, linear gullies whose heads are located close to the top of the mountain front (the rest of channels). In the centre of the mountain front, a number of drainage outlets of categories II and III (8 to 16 in Fig. 4a) are regularly spaced, which is a common feature in fault-induced mountain fronts.

Almost every longitudinal profile of the transverse stream channels shows one or two sharp gradient anomalies close to the fault trace, which are expressed by maxima of the Stream-gradient index (SL; Hack, 1973) that conspicuously stand out above the basal tendency. Anomalously high

SL values can be related to either highly resistant rocks or maladjustment of the channel profile due to recent tectonic activity or climatic changes (e.g. Keller and Rockwell, 1984; Burbank and Anderson, 2012). SL peaks induced by active faults use to be retreated at a distance upstream of the corresponding fault traces. In our case, most gradient anomalies either coincide with fault traces or are located downstream of them, which suggets that they are generally due to differential erosion of the Neogene soft materials in contact with Jurassic limestones, better than directly to tectonic movement. Two examples, corresponding to channels of categories I and III (numbers 8 and 18, respectively, in Fig. 4a), are illustrated in Figure 4b.

5.2. Displacement and slip rate

As mentioned in Section 4.2, activity of the Valdecebro fault zone initiated in the Late Ruscinian (mid Pliocene) and has remained till Late Pleistocene time. The throw for the last 3.7 Ma has been calculated by comparing the altitude of *FES* modelling the Corbalán block (1220 m) and that of the top of the correlative *Páramo 2* unit in the Valdecebro depression (1030 m); this renders a value of 190 m. Considering nearly pure dip-slip movement on an average 69º-dipping fault plane (see Section 4.2), the net slip would be ca. 205 m, and the net slip rate ca. 0.055 mm/a.

5.3. Preliminary seismogenic characterization

Considering a length of 5.2 km for the Valdecebro fault zone, and applying the empirical relationships proposed by Wells and Coppersmith (1994), Stirling *et al*. (2002), and Pavlides and Caputo (2004), we obtain potential moment magnitude M_w in the range of 5.8 to 6.4 for earthquakes generated by this structure. Concerning coseismic displacements, correlations proposed by Wells and Coppersmith (1994) and Pavlides and Caputo (2004) yield smaller values: maximum net slip of 0.18 m and 0.10 m, respectively; the correlation by Stirling *et al*. (2002) provides average coseismic slip of 0.34 m. Previous trench studies in the Teruel Graben show how in some cases (Concud fault; Lafuente *et al*., 2011a, 2014) the correlation model by Stirling *et al*. (2002) fits the measured coseismic slip values better than the other models, while in others (Teruel fault; Simón *et al*., 2017) the opposite occurs.

The potential moment magnitude Mw has also been approached from the seismic moment by using the equation proposed by Hanks and Kanamori (1979). In such a calculation, we have considered: (i) the average coseismic slip of 0.34 m obtained from Stirling's correlation (the results of our trench study will show that this is a realistic value); (ii) the rupture area expressed as the product of the trace length (5.2 km) and the fault width along dip (13-16 km, up to the detachment level below the brittle crust identified by Roca and Guimerà, 1992); and (iii) the average shear modulus μ commonly used for typical upper crustal rocks, $3\text{-}3.5 \cdot 10^{10}$ Pa. The resulting Mw ranges from 5.8 to 5.9.

6. Trench study

6.1. Location

The target for our paleoseismological study has been the southern branch of the Valdecebro fault zone at Los Huesares area, some 1.5 km north of Valdecebro village (see location in Figs. 2a and 3b). This branch crosses the Pleistocene pediment that comes from the main Valdecebro fault scarp, producing a conspicuous linear step with a slope close to 18% that strongly contrasts with the overall 3-6% slope of the pediment surface. The detailed profile of Figure 5a indicates that such topographic step could represent a vertical offset of ca. 6.5 m in the pediment surface. Field inspection has not shown any other evidence of surface rupture in Quaternary sediments on other branches at this sector of the Valdecebro fault zone. Therefore, we interpret that all (or most of) the displacement underwent since the Middle Pleistocene has been accommodated at this branch.

The trace of the studied fault branch can be recognized in a neighbouring gully located to the west, where red lutites of the *Rojo 3* or TN6 unit are put into contact with light orange gravel and silt of the pediment cover (Fig. 5b). The latter is strongly thickened (up to 8 m) with respect to the usual thickness observed in the footwall block (≈ 2 m).

A N030ºE trending, 40-m-long trench was dug across the topographic step. A total length of 29 m on its eastern wall was logged and analysed in detail, with a maximum depth at its central part exceeding 5 m (Fig. 6a).

6.2. Materials: lithology and sedimentology

Dug materials are entirely alluvial sediments representing the Pleistocene pediment cover. They have been subdivided into seven units; from bottom to top they are (Fig. 6a):

Unit 1: Whitish, yellowish and brown gravel with interbedded silt showing floating clasts, arranged in tabular levels. Gravel is grain-supported, with brown coarse sandy matrix and carbonate angular-subangular clasts, up to 15 cm in size, making dm-thick, finning-upward cycles.

Unit 2: Red gravel (withish towards the top) with interbedded cm-thick lensoid mudstone levels. Gravel is grain-supported with red matrix and mainly carbonate, angular-subangular clasts, up to 14 cm in size; they make tabular, dm-thick, finning-upward cycles. Units 1 and 2 can be interpreted as gravel bar deposits grown during waning water discharges.

Unit 3: Orange silt with floating granules and pebbles, up to 6 cm in diameter, deposited on a very irregular base. It represents lower energy flows onto the bar deposits of the underneath units.

Unit 4: Erosive channel filled by whitish, grey and brown gravel with interbedded irregular, orange silty levels. Gravel is matrix-free in the base, and shows increasing silty matrix towards the top, where some root traces are observed. Clasts are made of carbonate, angular to subrounded, up to 16 cm in size, making finning-upward cycles.

Unit 5: Alternating orange and whitish gravel and silty layers. Gravel is grain-supported, with orange sandy matrix. Clasts are made of carbonate, angular to subrounded, up to 12 cm in diameter, and form finning-upward cycles. Silty levels contain floating clasts up to 5 cm in size. Signs of pedogenesis, as root traces and carbonate nodules, are conspicuous. This unit was deposited under variable flow conditions, with episodic discharges of decreasing energy.

Unit 6: Matrix-supported gravel with angular-subangular carbonate clasts, up to 9 cm in size, in channelled, finning-upward levels. Root traces and carbonate nodules and crusts are recognized. Deposition of this unit is attributed to high density flows.

Unit 7: Regolith consisting of brown lutite with scattered centimetre-scale limestone clasts, carbonate nodules, and root traces.

Paleocurrent distribution, inferred from (i) axes of imbricated pebbles in units 1, 2 and 4, and (ii) trend of erosive channel in unit 4, is shown in Fig. 6c. Two relative maxima towards S and W can be distinguished in every unit and in both fault blocks. Southward paleocurrents are more conspicuous in unit 1, while westward ones dominate in unit 4 (including the channel trend).

6.3. Age model

The chronology of sedimentary units has been established applying OSL dating to six samples of silt to fine sand (Table 1). A total of 25 to 60 small multi-grain aliquots (approximately 10 grains per aliquot) of each sample were measured to determine the equivalent dose D_e. This aliquot size has proved to provide similar resolution as single grain measurements with the advantage of yielding a better signal to noise ratio (Medialdea *et al*., 2014). The resulting D_e population is normally distributed, with over-dispersion values (OD) below 20% for samples VALNORTE, VAL12E, VAL2C and VAL47F. Samples VAL45H and VAL9C are more widely scattered with OD values of 32% and 40%, respectively, suggesting that they were affected by incomplete bleaching, i.e. the mineral grains did not receive sufficient light exposure to reset their luminescence signal before being buried. The Central Age Model (CAM, Galbraith *et al*., 1999) has been used for the normally distributed dose populations from which the outliers (1.5 times the Inter Quartile Range) have been excluded. The Internal-External Consistency Criterion (IEU; Thomsen *et al*., 2007) has been applied to estimate the true burial dose of the incompletely bleached samples, VAL45H and VAL9A. This approach estimates the burial dose based on the dose values most likely to correspond to the well bleached population.

Dose rates have been calculated from the concentration of radionuclides measured by high resolution gamma spectroscopy on approximately 100 g of ground bulk material. Appropriate conversion factors (Guérin *et al*., 2011) were applied. A linear accumulation of deposits has been assumed in order to calculate the contribution of cosmic radiation according to a varying burial depth (based on Prescott and Hutton, 1994). The total dose rates were calculated according to attenuation caused by moisture and grain size. Water contents measured on each sample has been assumed representative of the burial time, with an added error of 2%. Total dose rates to an infinite matrix have been calculated using “DRAC calculator” (Durcan *et al*., 2015). The age adopted for each sample, as well as the paramenters necessary for its calculation, are summarized in Table 1.

On the basis of those numerical ages, taking into account vertical and lateral relationships of the sedimentary units (see Fig. 6a), and assuming constant accumulation rates for similar facies (higher for gravel, lower for lutite), we have elaborated a chronological model. First, we were compelled to discard the result of sample VALNORTE, owing to unavoidable contradiction with the sedimentary succession. Such an unreliable result could be due to extreme incomplete bleaching, meaning that the material sampled for this unit was not exposed to daylight at all during transport, therefore carrying a residual dose accumulated before last burial. Second, the aparent chronological inversion for samples VAL2C and VAL9A actually shows estimated ages which are compatible with sedimentary superposition if their associated error is taken into account: VAL9A could approach 121.1 + 7.6 = 128.7 ka BP, while VAL2C could approach 129.5 − 5.5 = 124.0 ka BP. The proposed age model, expressed as the most probable numerical age for the base of each unit, is the following:

- Unit 1: >149.1 ± 8.1 ka BP.
- Unit 2: close to the midway between 149.1 ± 8.1 and 136.2 ± 9.1 ka BP; we adopt 142 ka BP.
- Unit 3: sligthly older than 136.2 ± 9.1 ka BP; we adopt 137 ka BP.
- Unit 4: between 136.2 ± 9. and 128.7 ka BP, closer to the last age; we adopt 130 ka BP.
- Unit 5: sligthly older than 124.0 ka BP; we adopt 125 ka BP.
- Unit 6: bracketed between 124.0 and 50.1 ± 2.0 ka BP; we adopt 95 ka BP assuming constant accumulation rate.

6.4. Structural description and interpretation of paleoseismic events

We next describe in detail the faults and fractures exposed in the trench, their relationships with the sedimentary units, and hence we interpret the paleosesimic events and constrain their ages (Table 2). Three sectors (A, B and C in Fig. 6a) are analyzed separately, then correlations between them are established. Sectors A and C include two major extensional faults (ϕ and ε) responsible for the tectonic step observed in the Pleistocene pediment, as well as some associated, both synthetic and antithetic minor faults. Sector B corresponds to the block bounded by those main fault zones, which shows further deformation. Offsets (separations) measured along fault traces on the trench log are considered to closely approach net slip values, since the direction of the trench (azimuth: 030-210) is nearly parallel to the inferred transport direction (N202ºE; see Section 4.2).

6.4.1. Sector A

The oldest sedimentary body (Unit 1) is cut by fracture ρ (column 21 in Fig. 6a), which abruptly vanish at the base of Unit 2. It could therefore represent a first deformation event (Event A1; Table 2) with no visible.

Fault μ offsets the bases of units 2 and 3, while it is unconformably covered by the erosive base of Unit 5 (column 19; Fig. 6d). The measured offset, 0.4 m, could increase up to 0.6 m by adding the associated, gentle drag fold (Fig. 7). Therefore, a second event (Event A2; Table 2), later than Unit 3 and previous to Unit 5, can be defined. Fractures ω y θ, infiltrated with carbonate and also covered by Unit 5 (columns 22-23), could accompany this event; their unrooted character and almost negligible displacement suggest that they did not develop as independent structures.

Fracture band χ, made of two irregular walls confining destructured materials (columns 17-18 in Fig. 6a), should be interpreted as a tension fisure related to refraction at the extensional tip of a synthetic blind fault (horse-tail structure, in the sense of Granier, 1985). It consistently offsets (0.3 m; Fig. 7) the bases of units 2, 3 and 5, cutting up a sedimentary horizon 0.4 m above the base of Unit 5, where it dissapears (cell 17F). We can interpret that it moved during a single event coeval of the lower part of Unit 5 (Event A3, previous to deposition of the upper Unit 5; Table 2). However, considering that reactivation of the fault below unconsolidated materials might not propagate up to the surface, it could also occur post-Unit 5.

Faults ϕ and π (both connected at their upper segment and interrupted at the base of Unit 7; columns 19-20 in Fig. 6a) produce a net slip of 1.1 m at the base of Unit 2, while about 1.3 m at the bases of units 3 and 5 (Fig. 7). We can attribute such misft to the erosional character of the bases of units 3 and 5, which makes them less reliable as structural markers. In any case, such offset values are enough consistent for considering that they represent a single event younger than Unit 5 (Event A4; Table 2). We tentatively adopt a value of 1.1 m for the coseismic slip. The different kinematics and propagation style of fault ϕ with respect to fracture band χ suggest that both were activated in distinct deformation events.

The above explained four-event paleoseismic succession constitutes the optimum model for sector A according to the *Occam's razor* principle. Nevertheless, we should not throw out two complementary possibilities: (i) fault π (decoupled from fault ϕ) could have previously moved 0.1 m, either coeval of faults μ or χ (events A2 or A3) or during a previous (?) independent event (hypothetic Event A1'), which would reduce the coseismic slip of Event A4 to 1.0 m; (ii) Event 4 could be partitioned into two or more events younger than Unit 5 and older than Unit 7.

6.4.2. Sector B

Four faults, both synthetic (λ and σ) and antithetic (κ and η) to the major faults, appear at this sector. They define a narrow graben with the appearance of a double funnel in which unconsolidated gravel of Unit 4 has been sunk. Fault η has a shear component, as evinced by both offset of the base of Unit 4 and slikenlines measured at the rupture surface (plane: 093, 86 N; rake: 65 E; transport direction: N085ºE; Fig. 6b), but also a tensile component revealed by opening and filling with overlying material. The antithetic fault κ linked to λ is offset 0.15 m by fault σ (cell 10E in Fig. 6a). The accumulated net slip for the overall structure (synthetic slip on faults λ and σ minus anthitetic slip on η) is 0.5 m (Fig. 7). We can interpret that such displacement was accommodated during two deformation events occurred after deposition of Unit 4 (Table 2): Event B1, represented by a displacement of 0.35 m on fault λ, and Event B2, represented by a displacement of 0.15 m on fault σ. The anthitetic fault κ moved during Event B1, while η could be activated during both (probably as a shear rupture in B1 and a tensile fracture in B2).

6.4.3. Sector C

Fractures φ and τ are tension fractures infilled with white carbonate that covers and infiltrates their walls. They cut Unit 4 and are abruptly interrupted at the base of Unit 5 (column 2 in Fig. 6a), so they represent the oldest deformation event in this sector (Event C1; Table 2).

Fault β, anthitetic to the main fault ε, offsets 1.3 m the base of Unit 5 (column 26 in Fig. 6a), while only 0.1 m the base of Unit 6 (cell 5D). This indicates the occurrence of at least one event (Event C2; Table 2) intra-Unit 5 with an associated slip of 1.2 m on fault β (Fig. 7). Perhaps it was accompanied by slip on fault γ, which offsets >0.4 m the base of Unit 5 and vanish within this unit (column 26). We interpret that both antithetic faults represent brittle, rollover-like accommodation intrinsically linked to slip on fault ε. Therefore, a slip episode on that main fault ε, coeval of the lower Unit 5 and with coseismic slip exceeding 1.2-1.6 m, should also be attributed to Event C2. Combined slip on the synthetic fault ε (and δ?) and the antithetic faults β and γ created a narrow trough (columns 6-7) that was infilled with clastic materials belonging to Unit 5, which locally triple its average thickness.

Fault α (column 3; Fig. 6e) offsets 0.2 m the bases of units 5 and 6 (Fig. 7), and propagates up to a sedimentary horizon 0.5 m above the base of Unit 6 (dotted line H in Fig. 6a), where it abruptly dissapears. This allows attributing such slip to a single event, predated by the base of Unit 6 and posdated by the sedimentary horizon at the mid Unit 6 (Event C3; Table 2). Similar relationships have been observed for faults β and δ: they also offset 0.1-0.2 m the base of Unit 6 and are covered by the same sedimentary horizon H within Unit 6 (cells 5D and 7D). We can therefore infer that faults β and δ also underwent such slip during this Event C3 previous to deposition of the upper Unit 5. Owing to the same reasons above mentioned for faults β and γ, we interpret that the major fault ε (and δ?) should move under the same Event C3 (exceeding 0.3 m, in this case).

Slip on fault ε continued during and after deposition of Unit 6; this is entirely cut by that fault, and horizon H has undergone offset ≥ 2.3 m (Fig. 7). We should therefore identify at least one event younger than Unit 6 (Event C4; ≥ 2.3 m; Table 2), although, as in the case of fault ϕ, it could represent a composite of several events. The combined displacement of events C3 and C4 corresponds to the accumulated offset at the base of unit 6 (ca. 3.0 m). Finally, Unit 7 posdates this fault.

6.4.4. Syntesis and correlation

Faulting events interpreted in the three sectors are summarized in Table 2. Structures active in each of them, as well as their relative age and estimated coseismic slip, are indicated.

Each analyzed sector represents a fault zone which contributes to the total net displacement recorded at the trench: 2.0 m (sector A) + 0.5 m (sector B) + 4.5 m (sector C) = 7.0 m (Fig. 7, Table 2). The apparent vertical offset of the pediment surface, as estimated in Fig. 5, is ca. 6.5 m. This involves that this surface was essentially modelled before most of the structural offset was accomplished. The difference between both quantities (0.5 m) would represent the displacement previous to pediment modelling, which closely approaches the net slip associated to the only faulting event prior to Unit 5 (Event A2, fault μ). We therefore infer that the lowermost Unit 5 probably represented the sedimentary cover of the pediment while its modelling process was interrupted (ca. 124 ka BP), then being progressively offset by younger events. Such disruption constitutes an important millstone within the evolutionary model of the studied transect, which has been fully reconstructed using retrodeformational analysis (Fig. 8).

The optimum correlation guided by *Occam's razor* principle, expressed in Table 3, results in a paleoseismic succession made of seven events (T to Z). The criteria on which this correlation model is based are the following:

- Correlation A2-C1: Fractures φ and τ showing null displacement could be genetically linked to any broadly coeval fault. They have no effect on the slip history, and hence on the slip rate.
- Event A3 vs. C2: Fault ε and fracture band χ are considered as independient structures with distinct kinematics; ε is a surficial rupture during Event C2, while χ probably represents the upper segment of a blind fault. Displacements on them are therefore ascribed to different events. Their

relative chronology is based on the notion that the fracture band χ propagated below Unit 5.
- Correlation B1-C3 and B2-C4: Funnel-like structures observed in Sector B do not show the characteristic style of primary shear ruptures, neither splay fractures propagated from a blind fault. Better, they can be considered as secondary, oblique tension fissures, perhaps rooted at a fault since they accommodate a little vertical slip, but essentially induced by lateral unloading of the footwall block close to the fault scarp at sector C. Accordingly, events B1 (ruptures λ and κ) and B2 (ruptures σ and η) should be related to two successive, later episodes of movement on faults ε or δ (tentatively events C3 and C4, respectively).
- Event A4 vs. events C3 and C4: Events C3 and C4 on fault ε created the space in which the youngest syntectonic unit (Unit 6) was deposited. This suggests that these were the latest paleoseismic episodes recorded in the trench.

The chronological constrains for the proposed paleoseismic succession (including the most probable or tentative age assigned to each event according its confidence) and the resulting slip history are depicted in Figure 9. We should be aware on the uncertainties involved in this model, related to both inaccuracy of age bracketting and diversity of correlation criteria. We could adopt a more restrictive scenario, rigorously guided by *Occam's razor* principle, and consider e.g. structures ε and χ as related to the same event (merged A3+C2, V+W), the whole succession being therefore reduced to six events.

In contrast, a scenario of multiple events after comparing the coseismic slip values arising from the former ones with those obtained from empiric correlation (0.10-0.34 m; Section 5.3) could be preferred. Even if we (i) accept the highest value within that range, provided by Stirling's correlation, (ii) consider this is an average for the total fault trace, and (iii) assume a standard bell-shape for the slip-length distribution (e.g. Walsh and Watterson,1989), the maximum coseismic slip expectable at a given point of the Valdecebro fault zone should not exceed 0.7 m. Only three among six measured offsets (events U, W and Y) fit such an estimate, while the rest (events V, X and Z) are much larger (see Table 3). The 2.8-m-long coseismic slip attributed to Event Z is especially striking in this respect. This suggests that each of these 'bigger' slip episodes actually represents the sum of several successive events. Tentatively, Event V could be separated into two new events (V and V'), each one with coseismic slip ca. 0.7-0.8 m; Event X, into X and X', with coseismic slip ca. 0.5-0.6 m; and Event Z, into four new events (Z, Z', Z" and Z'") with coseismic slip ca. 0.7 m, all of them younger than ca. 80 ka but not necessarily younger than 50.1 ka.

According to the former alternative models of paleoseismic successions in the Valdecebro trench, the following average coseismic slip values and recurrence periods are inferred: (a) main model with seven events (T to Z): 100 cm, 15.3-23.7 ka; (b) model with six events (merged V+W):

117 cm, 18.4-28.4 ka; (c) model with twelve events (including V', X', Z', Z'', Z'''): 58 cm, 8.4-12.9 ka. On the other hand, the inferred local slip rate for the analyzed fault zone could range from 0.05 mm/a (considering the total lapse since 142 ka BP to the present) to 0.07 mm/a (considering only the time window recorded in the trench, i.e. assuming that the youngest event ocurred at this site ca. 50 ka BP) (Fig. 9b).

7. Interpretation and discussion

7.1. Paleoseismicity and slip rate of the Valdecebro fault zone within the framework of the regional active tectonics

The paleoseismic succession recorded at Los Huesares trench is made of a minimum of six-seven events, although a sequence of twelve events could represent a more realistic model. According to this variety of scenarios, the average coseismic slip would lie in the range of 58 to 117 cm, and recurrence periods in the range of 8.4 to 28.4 ka. A potential moment magnitude Mw = 5.8-5.9 can be assigned to such paleoearthquakes. Independently of which scenario is adopted, the local slip rate since 142 ka BP for the analyzed fault branch is reasonably constrained between 0.05 and 0.07 mm/a, similar to that recorded for the last 3.7 Ma (ca. 0.055 mm/a).

These values show some similarities an some differences with respect to those of the neighbouring Concud and Teruel faults (Table 4). Average coseismic slip in the shorter, Valdecebro and Teruel faults are consistently smaller than that of the longer Concud fault. Slip rate averaged for the last 3.5 Ma is similar for all faults (only sligthly lower in the case of Valdecebro); in contrast, for Late Pleistocene times it remains steady in the Valdecebro fault zone while strongly increases in the Concud and Teruel faults. In any case, we should not forget that this judgement is based on the notion that the fault branch exposed in Los Huesares trench actually accommodated all or most displacement of the Valdecebro fault zone since the Middle Pleistocene. We remind that no evidence of Quaternary activation of any other branch has been found at this sector.

Sequential fault activation and changes in fault slip rates can be interpreted in terms of progressive bulk 2D deformation accommodated within the studied area. Three successive stages can be envisaged within the evolving Neogene-Quaternary stress field proposed by e.g. Simón (1982, 1989), Arlegui *et al*. (2005), and Ezquerro (2017):

(1) Late Miocene. Onset of large N-S structures (La Hita fault zone) controlling basin initiation: prevailing E-W crustal stretching under a triaxial extension stress regime with W-E to WNW-ESE trending σ_3 trajectories.

(2) Since Early Pliocene, ca. 3.7-3.5 Ma. Activation of the E-W trending Valdecebro fault zone, together with the NW-SE Concud fault and the N-S Teruel fault: overall biaxial stretching under 'multidirectional' extension regime with WSW-ENE trending σ_3 trajectories.

(3) Late Pleistocene. Increasing slip rate in the Concud and Teruel faults, while the rate remains steady in the Valdecebro fault zone: although the tectonic conditions are essentially the same as in stage 2, bulk 2D deformation accelerates and becomes 'less biaxial', more anisotropic.

In summary, while the slip rates recorded at the Valdecebro, Concud and Teruel faults for longer timescales (3.5-3.7 Ma) are quite uniform (0.055 to 0.08 mm/a), short-term (Late Pleistocene) slip rates span a greater range (0.05-0.07, 0.29 and 0.19 mm/a, respectively) and attain significantly higher values in most of them. This represents a common situation in extensional fault systems, as documented by Mouslopoulou et al. (2009) in rifts of New Zealand, USA, Greece and Italy. On the other hand, over time scales of 10^4 to 10^5 years, the Concud and Teruel faults exhibit recent slip rates comparable to those on normal faults of more active regions in Spain as Betic Chains (e.g. Granada Fault: 0.03-0.38 mm/a, Baza Fault: 0.12-0.33 mm/a; Sanz de Galdeano *et al*., 2003; Alfaro *et al*., 2008; García-Tortosa *et al*., 2008); or in other active intraplate rifts around the world, such as northern Basin and Range (0.1 to 0.7 mm/a at Wasatch, West Valley, Oquirrh and Stansbury fault zones; Friedrich et al., 2003), San Luis Basin, New Mexico (0.10 mm/a at the Embudo fault zone; Bauer and Kelson, 2004), or lower Rhine Graben (0.07-0.3 mm/a; Meghraoui et al., 2000, and references therein). Slip rate on the Valdecebro fault zone is lower, which is consistent with its less favourable orientation with respect to the dominant ENE extension (Simón, 1989; Arlegui *et al*., 2005). Nevertheless, slip on this transverse structure has critically contributed to bulk deformation of the study area. Master, N-S striking faults were not able by themselves to enterely accommodate biaxial extensional deformation, and local switching σ_2 and σ_3 axes virtually led to activation of a E-W striking. This constitutes a typical case of stress/strain partitioning as defined by Simón *et al*. (2008), in which bulk biaxial extensional deformation is accomplished by slip on faults of diverse orientations driven by a non-linear sequence of local stress states within unvarying remote stress conditions.

Characterizing slip rate and paleoseismicity of the Valdecebro fault zone contributes to knowledge of active tectonics, and hence to seismic hazard assessment, of this area of the Iberian Chain. In spite of their structural and kinematic independence, mechanical interaction between Teruel and Concud faults has probably induced shortening of the seismic cycle; local stress perturbations caused by movement on one fault can trigger movement on the other one (Simón *et al.*, 2017). Average coseismic slip actually inferred from paleosesimic successions of the Concud and Teruel faults (7.1-8.0 and 16.7 ka, respectively; the latter one, only tentative) is smaller than that estimated from empirical correlation proposed by Villamor and Berryman (1999) using the average slip rate (ca. 11 and ca. 20 ka, respectively). Such comparison, although only represents a broad approach, plays in favour of the former hypothesis. In the same way, the presence of the neighbouring Valdecebro fault zone also should interfere with the Concud and Teruel faults, therefore causing further shortening of the interseismic period. In addition, seisms generated by the Valdecebro fault zone itself should be considered. The net result would be increasing of frequency, i.e. of probability of occurrence of seisms, although decreasing its maximum potential magnitude.

7.2. Structure and drainage rearrangement at the eastern margin of the Teruel basin

While activity of the eastern, N-S trending margin of the Teruel basin is documented since the beginning of the Late Miocene, the E-W trending Valdecebro fault zone undergoes displacement only since the late Ruscinian, in coincidence with the megasequential boundary B4 defined by Ezquerro (2017), ca. 3.7 Ma BP. Onset of the transverse Valdecebro fault zone, accompanying the intrabasinal, NNE-SSW striking Tortajada fault formerly developed (Ezquerro, 2017), outlined the triangle-shaped Corbalán block (Fig. 1), intermediate between the N-S trending La Hita fault zone and the basin floor, thus giving rise to strong rearrangement of the basin margin.

Also drainage patterns were rearranged as a consequence of structural changes (Fig. 10). During Late Miocene times, alluvial systems in both the Valdecebro and Corbalán sectors of the Teruel basin (*Rojo 1* unit) had been sourced at the eastern, active margin, as clearly indicated by recorded paleocurrents (Ezquerro, 2017) (Fig. 10a). By the end of the Miocene (ca. 6.1 Ma) the Tortajada fault was activated (Ezquerro, 2017); the alluvial systems remained functional on the Corbalán block, but their transport directions were reoriented towards the north and the south of the Tortajada fault (Fig. 10b). This suggests that the western, highest portion of the tilted Corbalán block (present-day Sierra Gorda range) represented a topographic barrier by that time.

By mid Pliocene time (top of *Rojo 2* unit, ca. 3.7 Ma) alluvial sedimentation on the Corbalán block was finally interrupted (Ezquerro, 2017) switching to erosional dismantling, while new southward drainage and sediment transport from the Corbalán block into the Valdecebro sector was triggered by activation of the transverse Valdecebro fault zone. This new drainage and sedimentary pattern persisted until mid Pleistocene times. Firstly, it resulted in building of very small alluvial fans belonging to *Rojo 2,* unit whose apical conglomeratic facies are observed close to the Valdecebro fault zone (Ezquerro, 2017) (Fig. 10c). During the Pliocene-Pleistocene transition, it partially contributed to the alluvial system linked to the *Villafranquian Pediment* (achieved ca. 2.1 Ma), although in this case the main source was located at the eastern margin (Cabezo Alto mountain front, La Hita fault zone; see Section 4.3) (Fig. 10d). During the Pleistocene, new alluvial systems were built from the Valdecebro mountain front, culminating at the southward slopping pediment surface (Fig. 10e).

Paleocurrents recorded in units 1, 2 and 4 of Los Huesares trench exhibit significant bimodality, indicating that both southward and westward drainage directions operate while the pediment developed in Middle Pleistocene times. Lack of connection between this pediment system and the Cabezo Alto mountain front makes unlikely that westward paleocurrents reflect regional drainage from the eastern basin margin. Better, they could be the result of channel reorientation in response to fault pulses at the transverse Valdecebro fault zone, which were coeval with deposition and should have influenced sedimentary supply/subsidence rate at the basin. West-directed flows, nearly parallel to the Valdecebro Fault, were probably subsequent to faulting events, when a gentle subsiding trough close to the fault trace could divert intrabasinal channels towards the W (e.g. channeled body in Unit 4 at the central sector of the trench, Fig. 6a). On the contrary, during periods of fault quiescence or abundant material supply the trough would be filled and the flows could overpass this gentle transverse trough and run free along the slope. With this respect, it is noteworthy that westward paleocurrents dominate in unit 4 (in contrast with previous units, in which southward ones are more conspicuous), i.e. close to the time when the earliest surficial faulting event was recorded in the studied trench (local Event A2; fault μ previous to Unit 5 in Fig. 6a). This suggests that any older tectonic pulse able to produce local flow reorientation was linked to a gentle accommodation monocline, easier to be overpassed by southward flow. Onset of surface rupture at Los Huesares was the key factor for increasing predominance of west-directed flows and, finally, for interrupting pediment formation ca. 124 ka BP (see Section 6.4).

Since that time, activity of the Valdecebro fault zone at Los Huesares branch has been persistent, at a rate that exceeds the capability of the alluvial system for remaining operational. Switch from southward to westward drainage in Unit 4 just was a precursor of the definitive, regional drainage change that occurred when the whole Valdecebro depression was incised by the Río Seco gully and captured by the Alfambra river (see Section 4.3) (Fig. 10f). Such capture, probably as a response to some important slip event in the Concud fault, occurred later than 124 ka and earlier than 22 ka BP.

8. Conclusions

The Valdecebro fault zone is an E-W trending, nearly pure extensional structure. It has accommodated a net slip of ca. 205 m since Late Ruscinian (Early Pliocene, ca. 3.7 Ma) to Late Pleistocene times, giving rise to a new transverse segment within the central sector of the N-S trending Teruel graben.

The paleoseismic succession at the Valdecebro fault zone, obtained from trenching at Los Huesares site, includes a minimum of six-seven events (T to Z) occurred since ca. 142 ka BP. Only the ages of the earliest ones (T and U) are well constrained, so that the duration of most interseismic periods is unknown. This paleoseismic succession embodies the activity recorded in a single fault branch, although it probably represents all or most of the displacement on this sector of the Valdecebro fault zone since Middle Pleistocene time. The total net displacement recorded at the trench is 7.0 m, most of it (6.5 m) subsequent to modelling of the Pleistocene pediment sourced at the Valdecebro scarp (ca. 124 ka BP). The resulting average coseismic slip (100-117 cm) clearly exceeds that expected from empiric correlation, which compel us to consider an alternative model including up to twelve events with average coseismic slip of 58 cm. According to the variety of scenarios, recurrence intervals could range from 8.4 to 28.4 ka. A potential moment magnitude Mw = 5.8-5.9 can be assigned to such paleoearthquakes.

The local slip rate inferred from trench analysis in the analyzed fault zone since 142 ka BP is constrained between 0.05 and 0.07 mm/a. This value is similar to that recorded for the last 3.7 Ma (ca. 0.055 mm/a) from offset of the *Fundamental Erosion Surface (FES)*, therefore suggesting a steady activity during the overall Pliocene-Pleistocene. This behaviour contrasts with that of the neighbouring NW-SE Concud and N-S Teruel faults, whose slip rate strongly increases during Late Pleistocene time (0.29 and 0.18-0.20 mm/a, respectively). Such activity pattern is consistent with the less favourable orientation of the Valdecebro fault zone with respect to the dominant ENE-WSW extensional trajectories of the stress field.

Drainage patterns were rearranged as a consequence of structural changes associated to the transverse Valdecebro fault activity: during Late Miocene (ca. 11-4 Ma), previous to the onset of Valdecebro structure, westward drainage from the eastern, original margin dominates; during Early Pliocene (3.7 Ma), activity of the Valdecebro fault zone and southward drainage from the Corbalán block initiates; during the Early Pleistocene (2.1 Ma) both drainage systems probably coexist, although westward drainage linked to the *Villafranquian Pediment* and sourced at the Cabezo Alto mountain front (La Hita fault zone) prevails; during the Middle Pleistocene, alluvial systems built from the Valdecebro mountain front culminate at a southward slopping pediment; subsequent to the onset of surface rupture at Los Huesares fault branch, and to the capture of the Valdecebro depression by the Alfambra river (between 124 and 22 ka BP), westward, axial drainage incised into the Valdecebro depression is established.

Acknowledgements

The research has been financed by project CGL2012-35662 of Spanish Ministerio de

Economía y Competitividad-FEDER, as well as by the Aragón regional government and the PO FEDER Aragón 2014-2020 (*Geotransfer* research group). We thank the Unit of Radioisotopes at the University of Seville for the OSL dating. We also thank Marta Ansón and Nausica Russo for helping us during field work and processing of trench photographs, respectively.

References

Alcalá L, Alonso-Zarza AM, Álvarez MA, Azanza B, Calvo JP, Cañaveras JC, van Dam JA, Garcés M, Krijgsman W, van der Meulen AJ, Morales J, Peláez P, Pérez-González A, Sánchez S, Sancho R, Sanz E (2000) El registro sedimentario y faunístico de las cuencas de Calatayud-Daroca y Teruel. Evolución paleoambiental y paleoclimática durante el Neógeno. Rev Soc Geol España 13:323–343

Alfaro P, Delgado J, Sanz de Galdeano C, Galindo-Zaldívar J, García-Tortosa FJ, López-Garrido AC, López-Casado C, Marín C, Gil A, Borque MJ (2008) The Baza Fault: a major active extensional fault in the Central Betic Cordillera (South Spain). Int J Earth Sci 97:1353–1365

Arlegui LE, Simón JL, Lisle RJ, Orife T (2005) Late Pliocene-Pleistocene stress field in the Teruel and Jiloca grabens (eastern Spain): contribution of a new method of stress inversion. J Struct Geol 27:693–705

Bai T, Maerten L, Gross MR, Aydin A (2002) Orthogonal cross joints: do they imply a regional stress rotation?. J Struct Geol 24:77–88

Bauer PW, Kelson K I (2004) Rift extension andfault slip rates in the southern San Luis Basin, New Mexico. In: Brister B, Bauer PW, Read AS, Lueth VW (eds) Geology of the Taos Region New Mexico, Geological Society 55th Annual Fall Field Conference Guidebook, pp 172-180

Bull WB, McFadden LD (1977) Tectonic Geomorphology north and south of the Garlock fault California. In: Doehring DO (ed) Geomorphology in arid regions. Allen & Unwin, London, pp 115–138

Burbank DW, Anderson RS (2012) Tectonic Geomorphology, Wiley-Blackwell, Oxford

Caputo R (1995) Evolution of orthogonal sets of coeval extension joints. Terra Nova 7:479–490

Caputo R (2005) Stress variability and brittle tectonic structures. Earth Sci Rev 70:103–127

Durcan JA, King GE, Duller GAT (2015) DRAC: Dose rate and age calculator for trapped charge dating. Quaternary Geochronology 28:54–61

Ezquerro L (2017) El sector norte de la cuenca neógena de Teruel: tectónica, clima y sedimentación. PhD Thesis, Universidad de Zaragoza

Ezquerro L, Luzón A, Navarro M, Liesa CL, Simón JL (2014) Climatic vs. tectonic signal in the Neogene extensional Teruel basin (NE Spain), based on stable isotope ($\delta^{18}O$) and megasequential evolution. Terra Nova 26:337–346

Ezquerro L, Moretti M, Liesa CL, Luzón A, Pueyo EL, Simón JL (2016) Controls on space-time distribution of soft-sediment deformation structures: approaching the apparent recurrence period of paleosisms at the Concud Fault (eastern Spain). Sedimentary Geology 344:91–111

Friedrich A M, Wernicke B P, Niemi NA, Bennett RA, Davis JL (2003) Comparison of geodetic and geologic data from the Wasatch region, Utah, and implications for the spectral character of Earth deformation at periods of 10 to 10 million years. Journal of Geophysical Research: Solid Earth, 108(B4), 2199, https://doi:10.1029/2001JB000682

Galbraith RF, Roberts RG, Laslett GM, Yoshida H, Olley JM (1999) Optical dating of single and multiple grains of quartz from Jinmium rock shelter, Northern Australia: part 1, experimental design and statistical models. Archaeometry 41:339–364

Garcés M, Krijgsman W, van Dam J, Calvo JP, Alcalá L, Alonso-Zarza AM (1999) Late Miocene alluvial sediments from the Teruel area: Magnetostratigraphy, magnetic susceptibility, and facies organization. Acta Geol Hisp 32:171–184

García-Tortosa FJ, Sanz de Galdeano C, Sánchez-Gómez M, Alfaro P (2008) Geomorphologic evidence of the active Baza Fault (Betic Cordillera, South Spain). Geomorphology 97:374–391

Godoy A, Ramírez JI, Olivé A, Moissenet E, Aznar JM, Aragonés E, Aguilar MJ, Ramírez del Pozo J, Leal MC, Jerez-Mir L, Adrover R, Goy A, Comas MJ, Alberdi MT, Giner J, Gutiérrez-Elorza M, Portero JM, Gabaldón V (1983) Mapa Geológico Nacional 1:50.000, Hoja 567 (Teruel). IGME, Madrid

Granier T (1985) Origin, damping, and pattern of development of faults in granite. Tectonics 4:721–737

Guérin G, Mercier N, Adamiec G (2011) Dose-rate conversion factors: update. Ancient TL 29(1):5–8

Gutiérrez F, Gutiérrez M, Gracia FJ, McCalpin JP, Lucha P, Guerrero J (2008) Plio-Quaternary extensional seismotectonics and drainage network development in the central sector of the Iberian Range (NE Spain). Geomorphology 102:21–42

Gutiérrez M, Peña JL (1976) Glacis y terrazas en el curso medio del río Alfambra (provincia de Teruel). Bol Geol Min 87:561–570

Hack JT (1973) Stream profile analysis and stream-gradient index. US Geol Surv J Res 1:421–429

Hanks TC, Kanamori H (1979) A moment magnitude scale. J Geophys Res 84:2348–2350

Herraiz M, De Vicente G, Lindo-Ñaupari R, Giner J, Simón JL, González-Casado JM, Vadillo O, Rodríguez-Pascua MA, Cicuéndez JI, Casas A, Cabañas L, Rincón P, Cortés AL, Ramírez M, Lucini M (2000) The recent (upper Miocene to Quaternary) and present tectonic stress distributions in the Iberian Peninsula. Tectonics 19:762–786

IGN (2017) Servicio de Información Sísmica del Instituto Geográfico Nacional. http://www.ign.es/ign/es/IGN/SisCatalogo.jsp. Accessed December 2017.

Kattenhorn SA, Aydin A, Pollard DD (2000) Joints at high angles to normal fault strike: an explanation using 3-D numerical models of fault-perturbed stress fields. J Struct Geol 22:1–23

Keller EA, Rockwell TK (1984) Tectonic geomorphology, Quaternary chronology and paleoseismicity. In: Costa JE, Fleisher PJ (eds) Development and Applications of Geomorphology. Springer, Berlin, pp 203–239

Lafuente P (2011) Tectónica activa y paleosismicidad de la falla de Concud (Cordillera Ibérica central). PhD Thesis, Universidad de Zaragoza

Lafuente P, Arlegui LE, Liesa CL, Simón JL (2011a) Paleoseismological analysis of an intraplate extensional structure: the Concud fault (Iberian Chain, Spain). Int J Earth Sci 100:1713–1732

Lafuente P,. Arlegui LE, Casado I, Ezquerro L, Liesa CL, Pueyo Ó, Simón JL (2011b) Geometría y cinemática de la zona de relevo entre las fallas neógeno-cuaternarias de Concud y Teruel (Cordillera Ibérica). Rev Soc Geol España 24:117–132

Lafuente P, Arlegui LE, Liesa CL, Pueyo Ó, Simón JL (2014) Spatial and temporal variation of paleoseismic activity at an intraplate, historically quiescent structure: the Concud fault (Iberian Chain, Spain). Tectonophysics 632:167–187

McCalpin JP (1996) Paleoseismology. Academic Press, New York

Medialdea A, Thomsen KJ, Murray AS, Benito G (2014) Reliability of equivalent-dose determination and age-models in the OSL dating of historical and modern palaeoflood sediments. Quaternary Geochronology 22:11–24

Meghraoui M, Camelbeeck T, Vanneste K, Brondeel M, Jongmans D (2000) Active faulting and paleoseismology along the Bree fault, lower Rhine graben, Belgium. Journal of Geophysical Research: Solid Earth 105(B6):13809-13841

Moissenet E (1993) L'age et les déformations des terrases alluviales du Fossé de Teruel. In: El Cuaternario de España y Portugal. IGME-AEQUA, Madrid, pp 267–279

Mouslopoulou V, Walsh JJ, Nicol A (2009) Fault displacement rates on a range of timescales. Earth Planet Sci Lett 278:186-197

Murray AS, Wintle AG (2003) The single aliquot regenerative dose protocol: potential for improvements in reliability. Radiation Measurements 37:377–381

Pavlides S, Caputo R (2004) Magnitude versus faults´ surface parameters: quantitative relationships from the Aegean Region. Tectonophysics 380:159–188

Peña JL (1981) Las acumulaciones cuaternarias de la confluencia de los ríos Alfambra y Guadalaviar, en las cercanías de Teruel. Actas VII Coloquio de Geografía, Pamplona, pp 255–259

Peña JL, Gutiérrez M, Ibáñez M, Lozano MV, Rodríguez J, Sánchez M, Simón JL, Soriano MA, Yetano LM (1984) Geomorfología de la provincia de Teruel. Instituto de Estudios Turolenses, Teruel

Prescott JR, Hutton JT (1994) Cosmic ray contributions to dose rates for luminescence and ESR: large depths and long-term time variations. Radiation Measurements 23:497–500

Roca E, Guimerà J (1992) The Neogene structure of the eastern Iberian margin: structural constraints on the crustal evolution of the Valencia trough (western Mediterranean). Tectonophysics 203:203–218

Sánchez Fabre M (1989) Estudio geomorfológico de la Depresión de Alfambra-Teruel-Landete y sus rebordes montañosos. PhD Thesis, Universidad de Zaragoza

Sanz de Galdeano C, Peláez JA, López-Casado C (2003) Seismic potential of the main active faults in the Granada Basin (Southern Spain). Pure and Applied Geophysics 160:1537–1556

Simón JL (1982) Compresión y distensión alpinas en la Cadena Ibérica Oriental. PhD Thesis, Universidad de Zaragoza (publ. Instituto de Estudios Turolenses, Teruel, 1984)

Simón JL (1983) Tectónica y neotectónica del sistema de fosas de Teruel. Teruel 69:21–97

Simón JL (1989) Late Cenozoic stress field and fracturing in the Iberian Chain and Ebro Basin (Spain). J Struct Geol 11:285-294

Simón JL, Serón FJ, Casas AM (1988) Stress deflection and fracture development in a multidirectional extension regime. Mathematical and experimental approach with field examples. Annales Tectonicae 2: 21–32

Simón JL, Arlegui LE, Liesa CL (2008) Stress partitioning: a practical concept for analysing boundary conditions of brittle deformation. Geodinamica Acta 53:1057–1065

Simón JL, Arlegui LE, Ezquerro L, Lafuente P, Liesa CL, Luzón A (2016) Enhaced paleoseismic succession at the Concud Fault (Iberian Chain, Spain): new insights for seismic hazard assessment. Natural Hazards 80:1967–1993

Simón JL, Arlegui LE, Ezquerro L, Lafuente P, Liesa CL, Luzón A (2017) Assessing interaction of active extensional faults from structural and paleoseismological analysis: The Teruel and Concud faults (eastern Spain). J Struct Geol 103:100–119

Stirling M, Rhoades D, Berryman K (2002) Comparison of Earthquake Scaling Relations Derived from Data of the Instrumental and Preinstrumental Era. Bull Seismol Soc Am 92:812-830

Thomsen KJ, Murray AS, Bøtter-Jensen L, Kinahan J (2007) Determination of burial dose in incompletely bleached fluvial samples using single grains of quartz. Radiation Measurements 42:370–379

Villamor P, Berryman KR (1999) La tasa de desplazamiento de una falla como aproximación de primer orden en las estimaciones de peligrosidad sísmica. I Congreso Nacional de Ingeniería Sismica, Asociación Española de Ingeniería Sísmica, Abstracts 1.

Walsh JJ, Watterson J (1989) Displacement gradients on fault surfaces. J Struct Geol 11:307–316

Wells DL, Coppersmith KJ (1994) New Empirical Relationships among Magnitude, Rupture Length, Rupture Width, Rupture Area, and Surface Displacement. Bull Seismol Soc Am 84:974–1002

FIGURE CAPTIONS

Fig. 1. Location of the Valdecebro fault zone (VFZ) within the Teruel graben system, eastern Spain. Inset: sketch of the main Alpine chains within the Iberian Peninsula.

Fig. 2. (a) Geological map of the Valdecebro fault zone and its surrounding area. Genetic units (TN1 to TN 6) defined by Ezquerro (2017) are mapped. Stars locate mesostructural data sites compiled in d. LHT: location of Los Huesares trench. (b) Correlation of those units with informal lithological units defined by Godoy et al. (1983). (c) Equal-area plot (lower hemisphere) showing orientations of measured planes and a slickenline on fault surfaces. (d) Cross-section of the Valdecebro fault zone (see location in a).

Fig. 3. (a) Morphotectonic map of the Valdecebro depression and surrounding reliefs. (b) Partial view of the Pleistocene pediment sourced at the Valdecebro fault mountain front. The arrows show the slope anomaly through which the paloseismological trench was excavated. (c) Topographic profile across the Valdecebro depression (see location in a), which shows altitudinal continuity between pediment surfaces north and south of the Río Seco gully (vertical scale x2.5).

Fig. 4. (a) Digital Elevation Model (DEM) of the northern margin of the Valdecebro depression, showing the transverse drainage network (stream channels numbered 1 to 22). DEM: pixel: 5 x 5 m; year: 2012; Instituto Geográfico de Aragón, http://idearagon.aragon.es/. (b) Two examples of longitudinal profiles and the corresponding curves of variation of the Stream-gradient index (SL) along channels transverse to the Valdecebro fault mountain front (numbers 8 and 18 in a); the position of fault traces is indicated.

Fig. 5. (a) Topographic profile across the anomalous step observed in the Pleistocene pediment surface, where the paleoseismological trench was dug (vertical scale x2.5). (b) Field view of the pediment profile, offset by the fault cropping out in a neighbouring gully.

Fig. 6. (a) Detailed log of Los Huesares trench. 1, 2, 3, 4, 5, 6, 7: Quaternary units described in the text; light-grey stripes: carbonate; Fθ, Fω, Fρ ... Fφ: faults referred in the text. The location and age of samples dated by OSL is indicated. Black: OSL age considered for paleoseismic reconstruction; grey: non-reliable age. (b) Rose diagrams of paleocurrents inferred from imbricate pebbles in sedimentary units 1, 2 and 4; the arrow depicts the direction of the big erosive channel in unit 4. (c) Stereoplot (equal area, lower hemisphere) of fault planes and slickenlines measured within the trench. (d) and (e) Detail view of three cells (3B, 19F, 19G) within the trench wall.

Fig. 7. Schematic log showing measurements of partial and total net slip on faults of the three analyzed sectors of Los Huesares trench (see text for details).

Fig. 8. Evolutionary model of sedimentation and deformation recorded at the Valdecebro trench

from retrodeformational analysis. Each sketch represents a stage subsequent to the paleoseismic event (and, in some cases, deposition of sedimentary units) labelled above.

Fig. 9. (a) Chronological sketch of paleoseismic events recorded at the Valdecebro trench according to the optimum correlation model. (b) Slip history based on the optimum correlation model (black line), on a more restrictive scenario that merges events V and W (grey line), and on a multi-event scenario that considers smaller, perhaps more realistic coseismic slip values (blue line).

Fig. 10. Evolutionary model of structure and drainage rearrangement at the central sector of the eastern Teruel Basin during Late Miocene to present times. Sedimentation areas (coloured), alluvial systems, paleocurrents (blue arrows) and active faults are depicted in each sketch. See text for details.

TABLE CAPTIONS

Table 1. Parameters and results of OSL dating of samples collected at the Valdecebro trench. H: hanging wall block; F: footwall block.

Table 2. Summary of paleoseismic events interpreted at sectors A, B and C of the Valdecebro trench.

Table 3. Summary of paleoseismic events correlated all along Los Huesares trench according to the more probable scenario guided by the *Occam's razor* principle. Age constraints are based on the central OSL numerical ages (without considering error bars; in ka with decimals), and the adopted ages according to the age model explained in Section 6.3 (in ka without decimals).

Table 4. Comparison of kinematic and paleosesismic parameters of the Valdecebro, Concud and Teruel faults.

Figure 1

Click here to download Figure Fig 1.tif

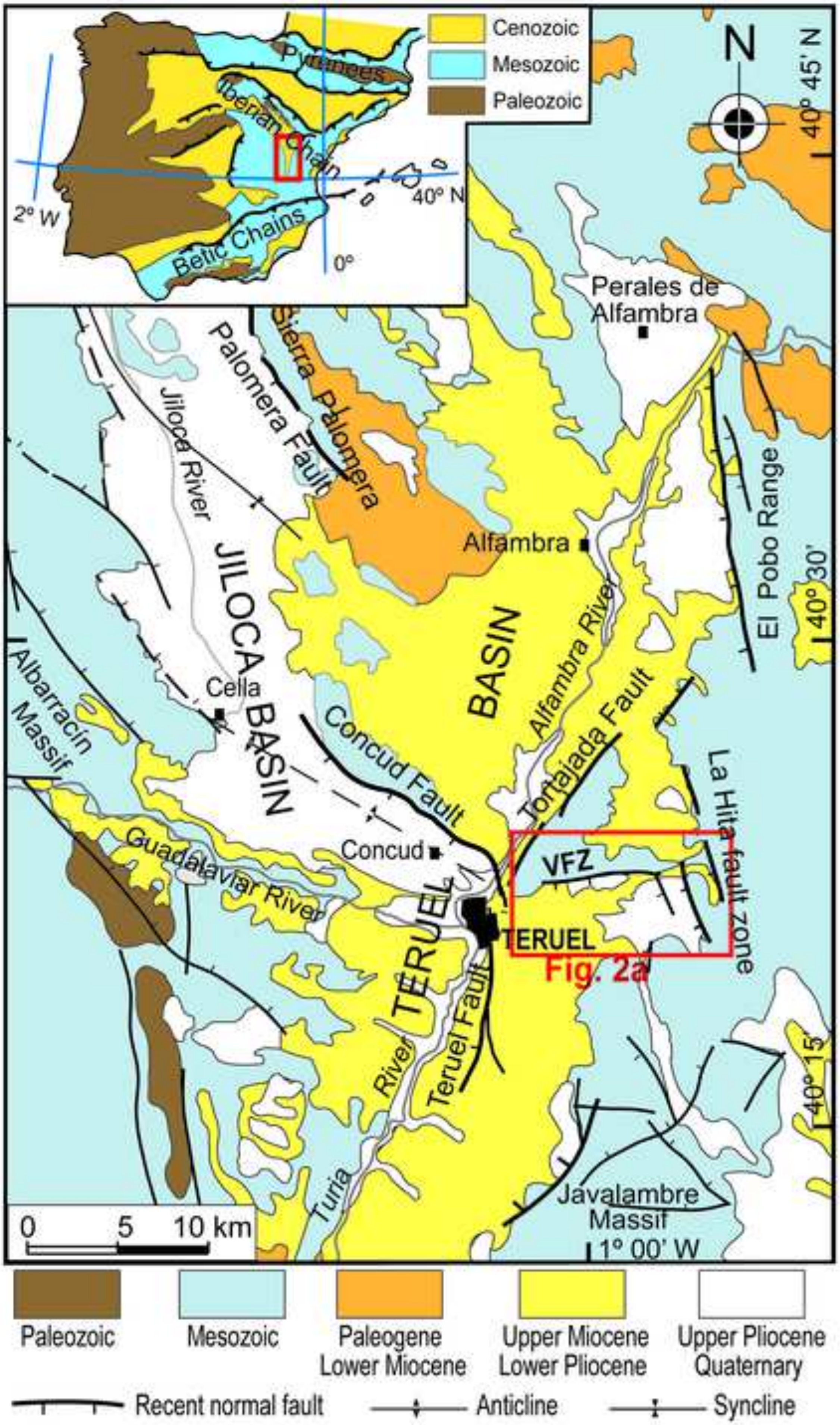

Figure 2

Click here to download Figure Fig 2.tif

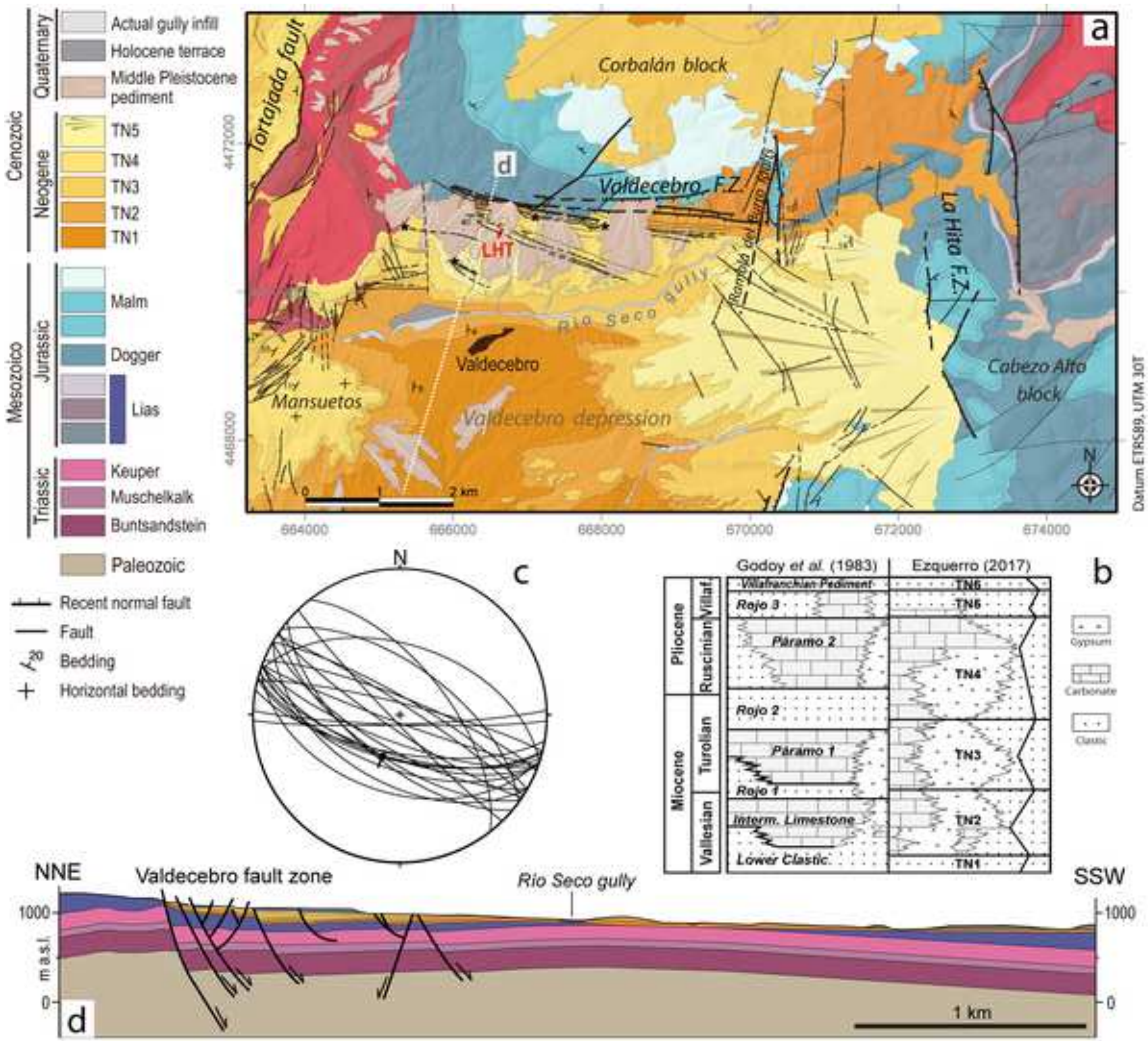

Figure 3

Click here to download Figure Fig 3.tif

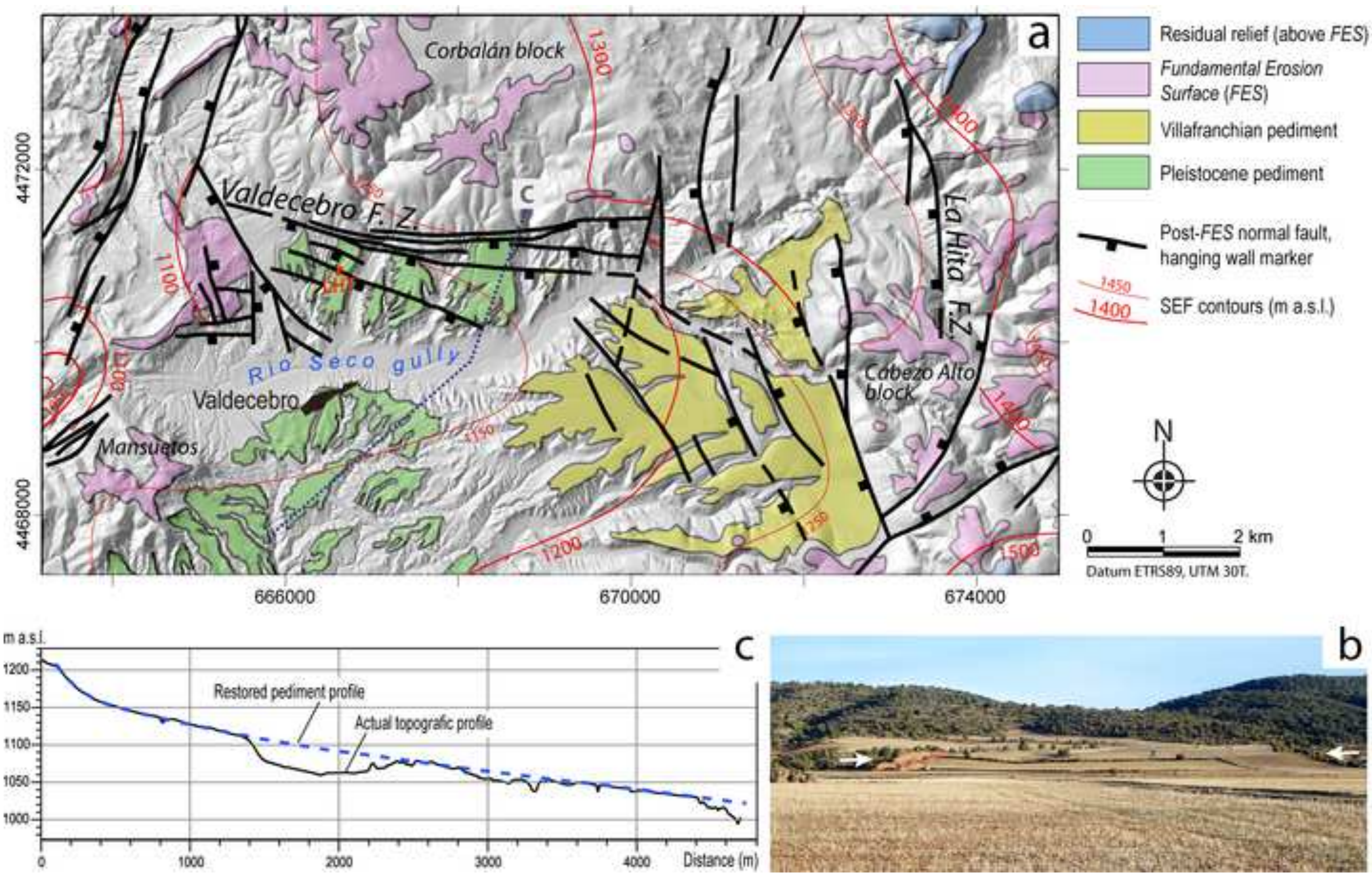

Figure 4

Click here to download Figure Fig 4.tif

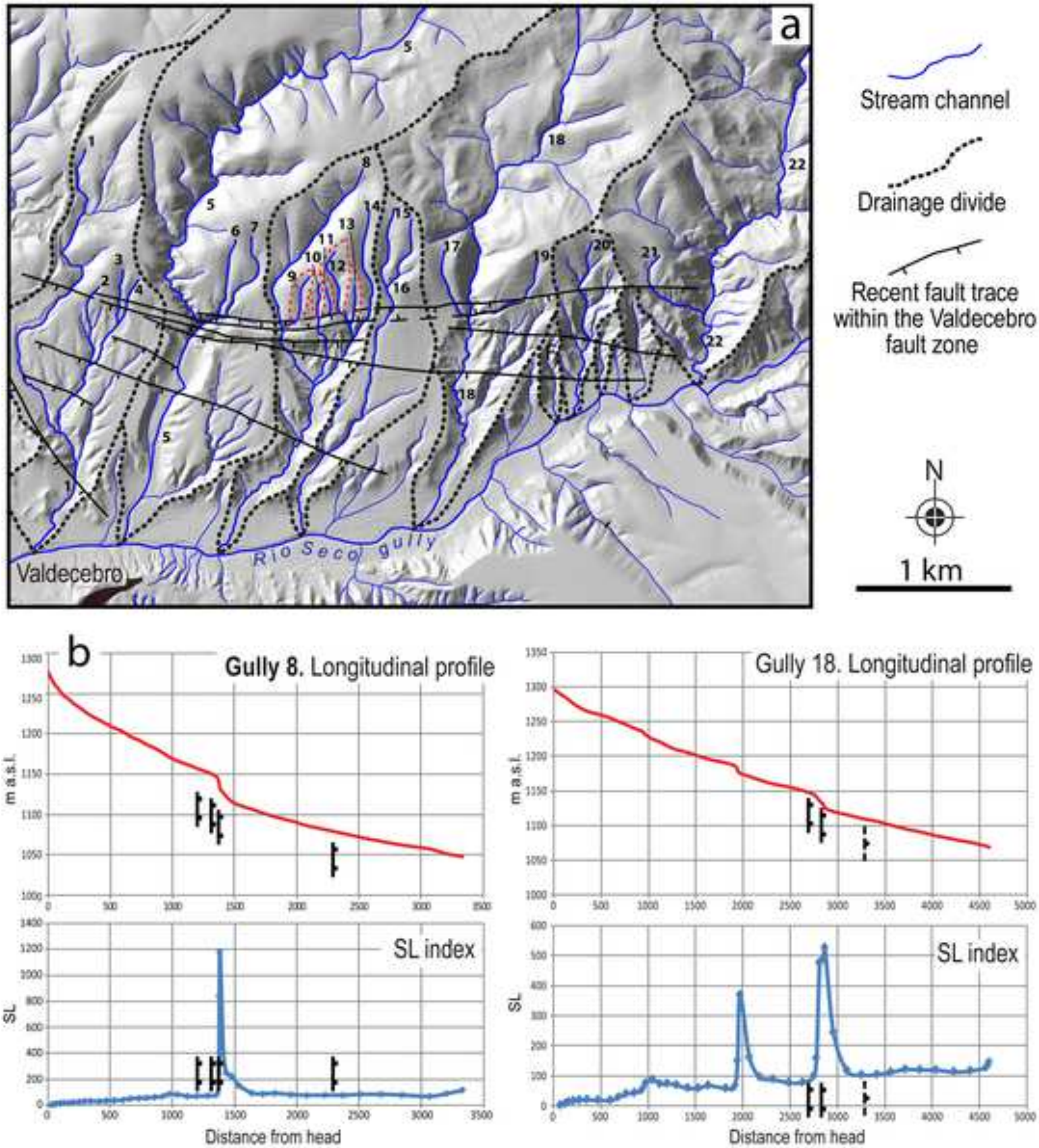

Figure 5

Click here to download Figure Fig 5.tif

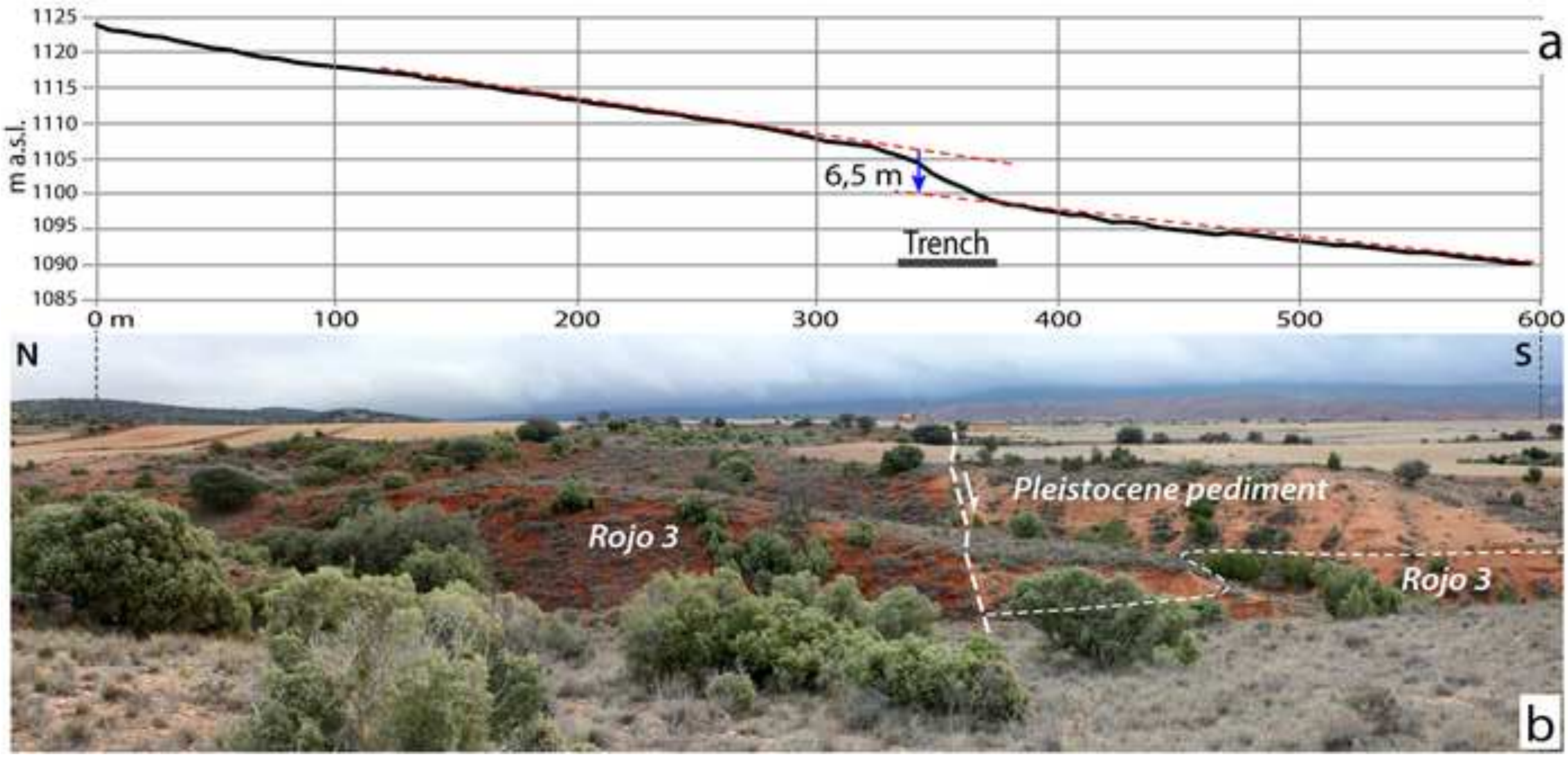

Figure 6

Click here to download Figure Fig 6.tif

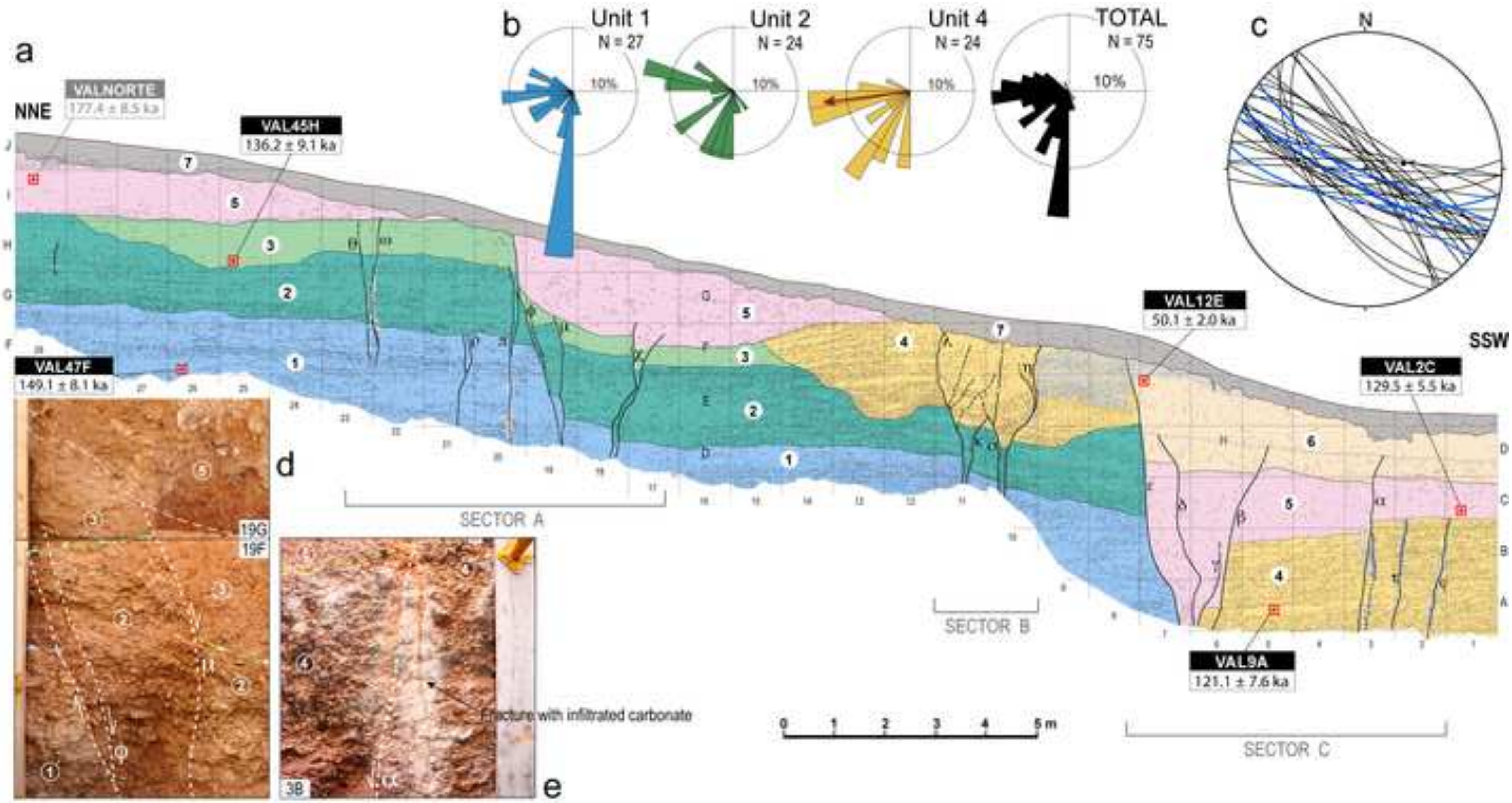

Figure 7

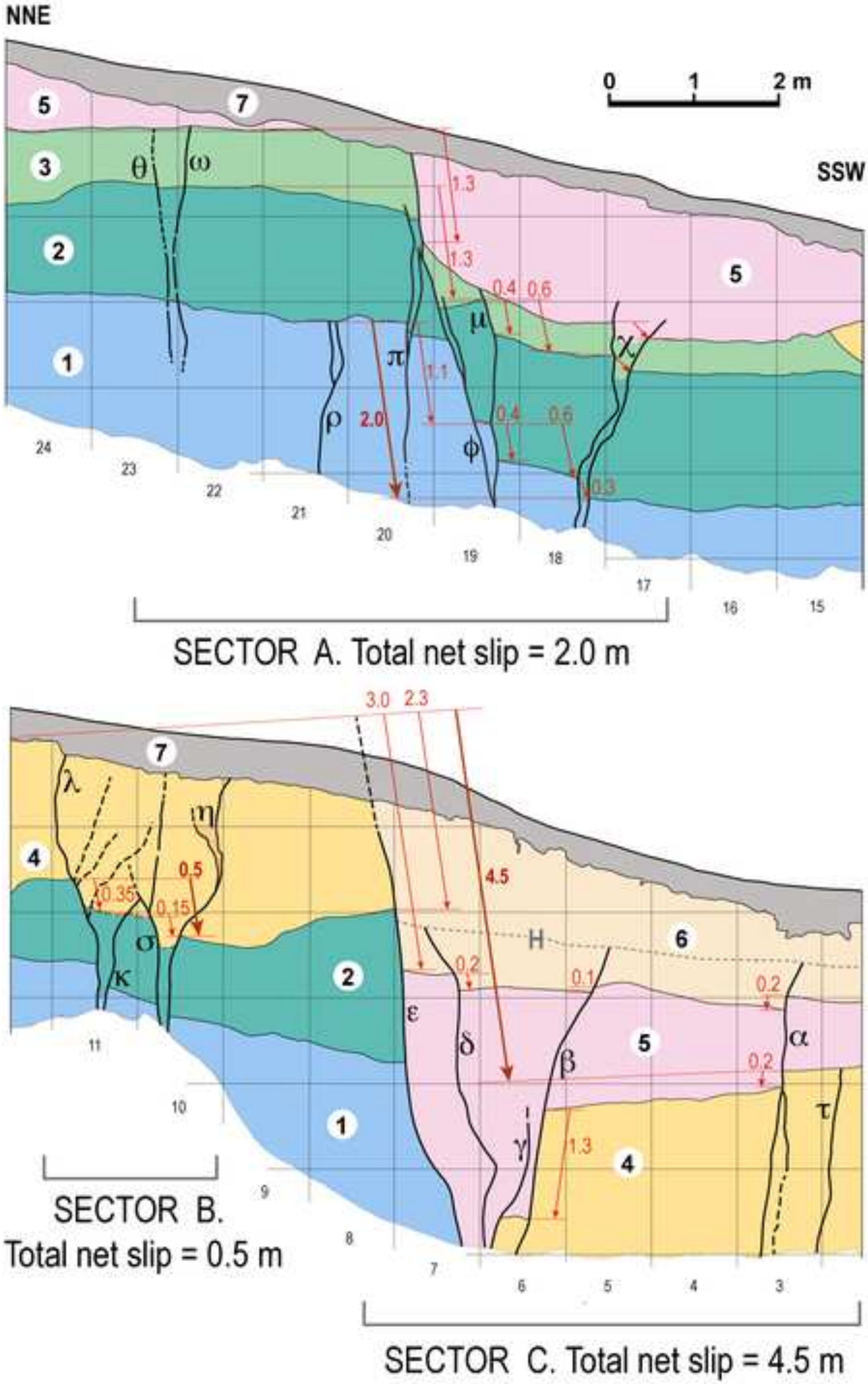

NNE
SSW
0 1 2 m
5
7
3
θ
ω
2
1
1.3
1.3
0.4 0.6
μ
χ
π
1.1
ρ
2.0
0.4 0.6
φ
0.3
24
23
22
21
20
19
18
17
16
15
SECTOR A. Total net slip = 2.0 m
3.0 2.3
7
λ
η
4
0.5
0.35
0.15
σ
κ
4.5
H
6
2
0.2
0.1
0.2
ε
δ
5
β
α
0.2
1
γ
τ
1.3
4
11
10
9
8
7
6
5
4
3
SECTOR B.
Total net slip = 0.5 m
SECTOR C. Total net slip = 4.5 m

Figure 8

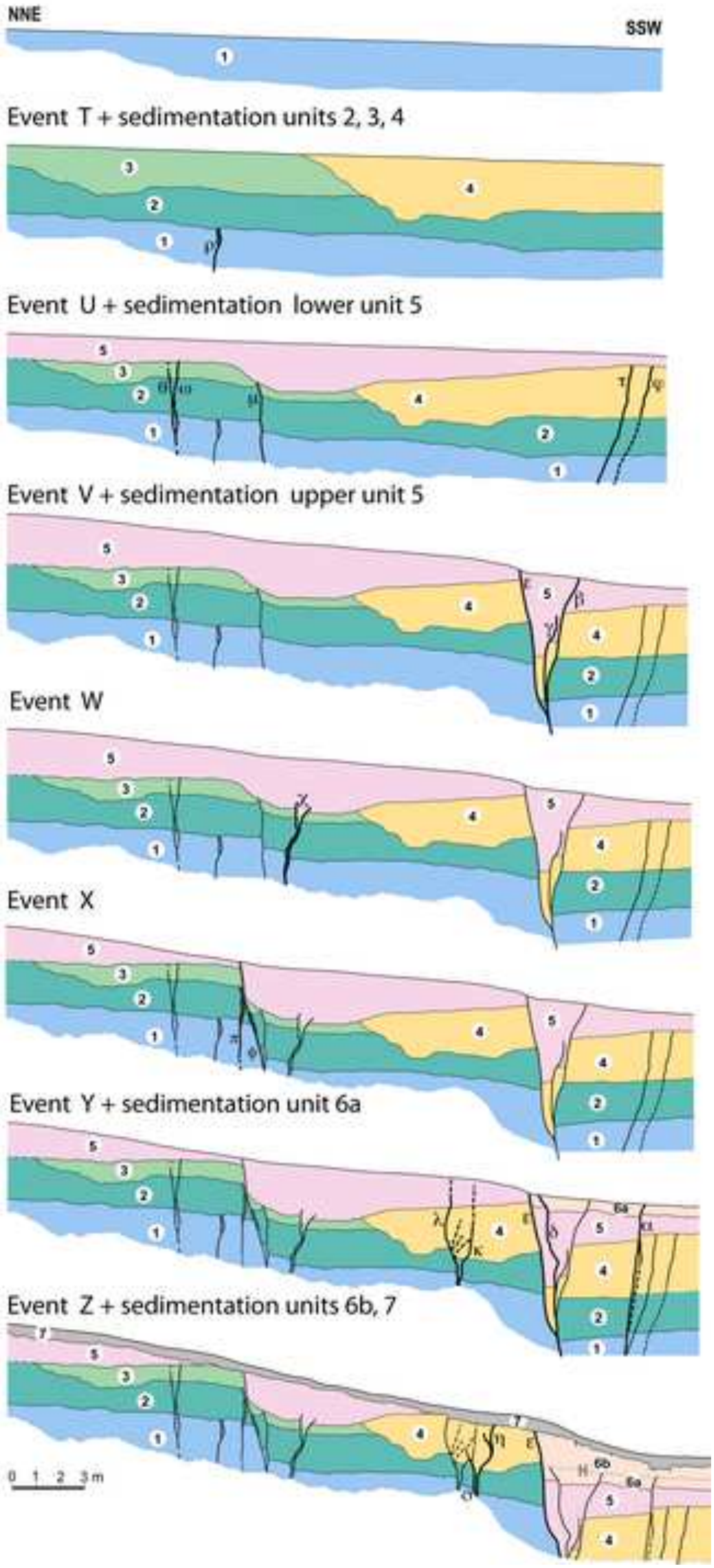
NNE
SSW
Event T + sedimentation units 2, 3, 4
Event U + sedimentation lower unit 5
Event V + sedimentation upper unit 5
Event W
Event X
Event Y + sedimentation unit 6a
Event Z + sedimentation units 6b, 7
0 1 2 3 m

Figure 9

Click here to download Figure Fig 9.tif

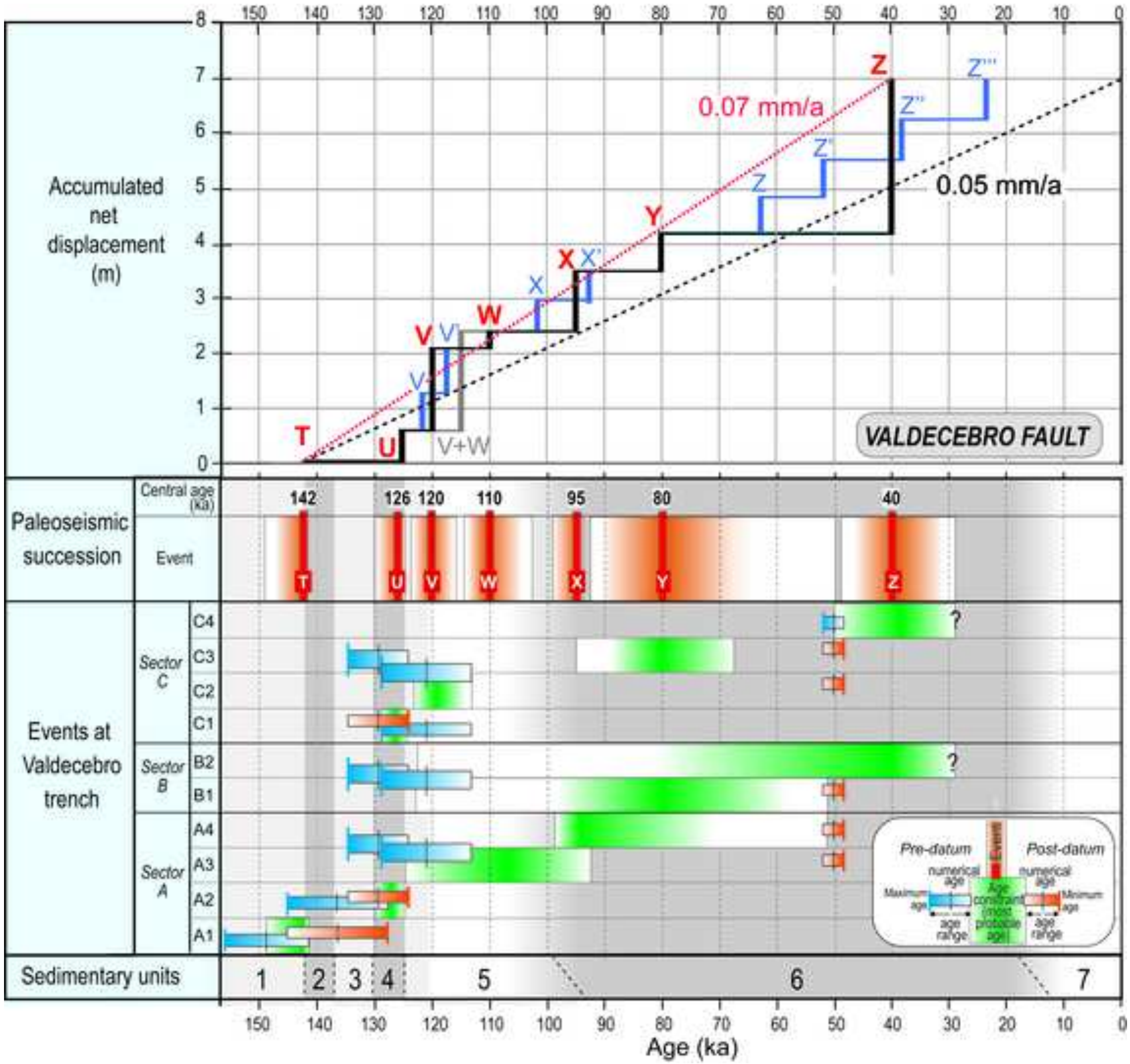

Figure 10

Click here to download Figure Fig 10.tif

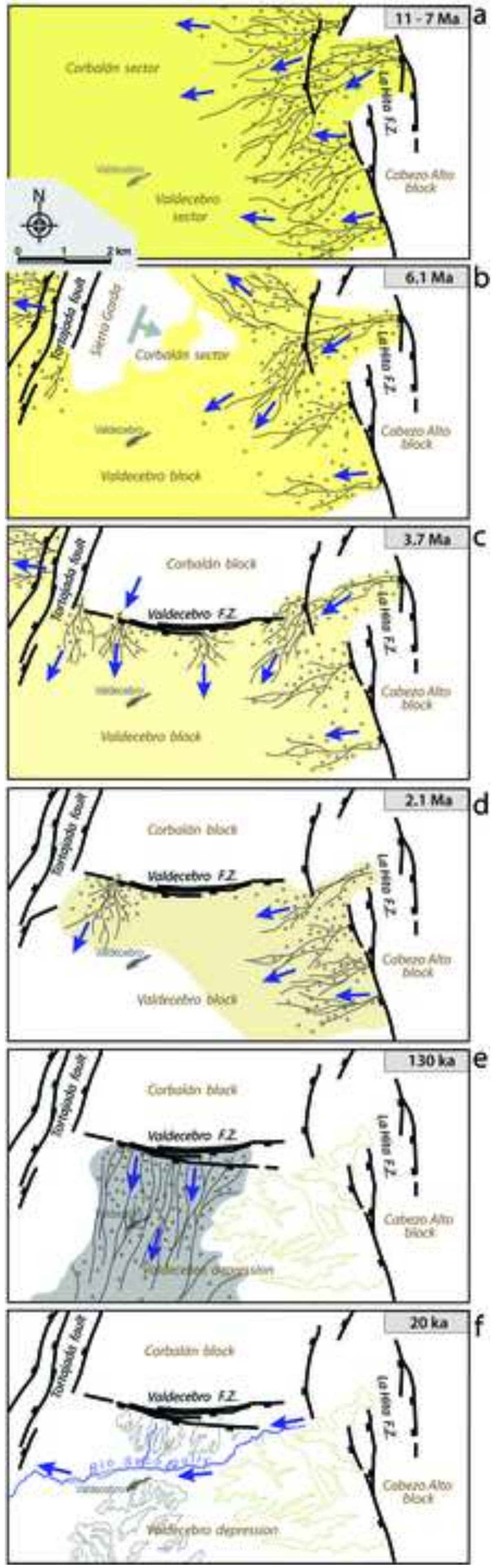

Table 1

Sample	Geographical -geological location	Stratigraphic location	Depth (m)	Water (%)	^{40}K (Bq/kg)	^{232}Th (Bq/kg)	^{238}U (Bq/kg)	Dose rate (Gy/ka)	Equivalent dose (Gy)	Age (ka)
VAL12E	SSW (H)	Unit 6 (top)	0.60	4	212 ± 10	27 ± 2	18 ± 1	1.68 ± 0.05	84.0 ± 2.1	50.1 ± 2.0
VAL2C	SSW (H)	Unit 5 (base)	1.40	4	223 ± 12	23 ± 1	13 ± 1	1.53 ± 0.05	197.7 ± 5.8	129.5 ± 5.5
VAL9A	SSW (H)	Unit 4 (middle)	4.10	4	217 ± 10	22 ± 1	11 ± 1	1.41 ± 0.04	170.1 ± 9.5	121.1 ± 7.6
VALNORTE	NNE (F)	Unit 5 (middle)	0.60	4	127 ± 10	12 ± 1	9 ± 1	0.99 ± 0.04	168.1 ± 5.2	170.4 ± 8.5
VAL45H	NNE (F)	Unit 3 (base)	1.90	7	271 ± 12	27 ± 1	14 ± 1	1.69 ± 0.05	230.6 ± 14.0	136.2 ± 9.1
VAL47F	NNE (F)	Unit 1 (middle)	3.80	10	298 ± 13	30 ± 1	16 ± 1	1.77 ± 0.05	264.0 ± 12.4	149.1 ± 8.1

Table 1. Parameters and results of OSL dating of samples collected at the Valdecebro trench. H: hanging wall block; F: footwall block.

Table 2

Event	Relative age	Structures	Net slip, structure (m)	Net slip, event (m)	
Sector A					
A1	Post Unit 1 – pre Unit 2	Fracture ρ	0	0	
A2	Post Unit 3 – pre Unit 5	Fault μ	0.6	0.6	
		Fractures ω, θ	0		
A3	Sin?-post? Unit 5	Fracture band χ	0.3	0.3	
A4	Post Unit 5 – pre Unit 7	Faults ϕ, π	1.1	1.1	
			Accumulated net slip in Sector A	***2.0***	
Sector B					
B1	Post Unit 4 – pre Unit 7	Fault λ	0.35	0.35	
		Antithetic fault κ	0		
		Antithetic fault η	- ?		
B2	Post Unit 4 – pre Unit 7	Fault σ	0.35	0.15	
		Antithetic fault η	- 0.2?		
			Accumulated net slip in Sector B	***0.5***	
Sector C					
C1	Post Unit 4 – pre Unit 5	Fractures φ, τ	0	0	
C2	Sin lower Unit 5	Fault ε (δ?)	>1.2 (>1.6?)	1.5	
		Antithetic fault β	- 1.2		
		Antithetic fault γ	- 0.4?		
C3	Sin lower Unit 6 (Pre horizon H)	Fault ε (δ?)	> 0.3	?	
		Antithetic faults α, β	- 0.3		3.0
C4	Post Unit 6 – pre Unit 7	Fault ε	≥ 2.3	≥ 2.3	
			Accumulated net slip in Sector C	***4.5***	
			Total accumulated net slip	**7.0**	

Table 2. Summary of paleoseismic events interpreted at sectors A, B and C of the Valdecebro trench.

Table 3

Events at sectors			Correlated events at Los Huesares trench				
A	**B**	**C**	**Event**	**Net slip (m)**	***Age constraints***		**Event age (ka)**
					Relative age	**Numerical age (ka)**	
A1			T	0.0 (A)	Post Unit 1 – pre Unit 2	149.1 - 142	142 (A)
A2		C1	U	0.6 (A)	Post Unit 3 (4?) – pre Unit 5	130 - 125	126 (A)
		C2	V	1.5 (B)	Sin lower Unit 5	Post 125	120 (B)
A3			W	0.3 (A)	Sin?-post? Unit 5	Post 125	110 (B)
A4			X	1.1 (A)	Post Unit 5 – pre Unit 7	Post 125	95 (B)
	B1	C3	Y	0.7 (B)	Sin lower Unit 6	95 – 50.1	80 (B)
	B2	C4	Z	2.8 (B)	Post Unit 6 – pre Unit 7	Post 50.1	40 (B)
2.0	**0.5**	**4.5**		**7.0** (A)	**← Total net slip (m)**		

(A) More probable values
(B) Tentative values

Table 3. Summary of paleoseismic events correlated all along Los Huesares trench according to the more probable scenario guided by the *Occam's razor* principle. Age constraints are based on the central OSL numerical ages (without considering error bars; in ka with decimals), and the adopted ages according to the age model explained in Section 6.3 (in ka without decimals).

Table 4

Fault	**Valdecebro**	**Concud** ([A])	**Teruel** ([B])
Average coseismic slip (cm)	58 - 117	190	50 - 57
Recurrence period (ka)	8.4 - 28.4	7.1 - 8.0	(16.7)
Net slip rate 74-142 ka (mm/a)	0.05 - 0.07	0.29	0.18 - 020
Net slip rate 3.5-3.7 Ma (mm/a)	0.055	0.07 - 0.08	0.075
Transport direction	N202ºE	N220ºE	N275ºE
Length (km)	5.2	14.2	9.0
Mw	5.8 - 5.9	6.6 - 6.8	6.1 - 6.6

([A]) After Lafuente (2011), Lafuente *et al*. (2011a,b, 2014), Simón *et al*. (2016)
([B]) After Simón *et al*. (2017)

Table 4. Comparison of kinematic and paleosesismic parameters of the Valdecebro, Concud and Teruel faults.